UNIVERSIDADE FEDERAL DO CEARÁ
FACULDADE DE MEDICINA

Reinaldo B. Oriá, DVM, PhD

Cryptosporidiosis as a model of environmental gut-brain axis dysfunction

C. parvum oocysts

20.0 µm

Laboratório da Biologia da Cicatrização, Ontogenia e Nutrição de Tecidos

https://labiconte.ufc.br
E-mail: oria@ufc.br

Localize-nos no mapa:

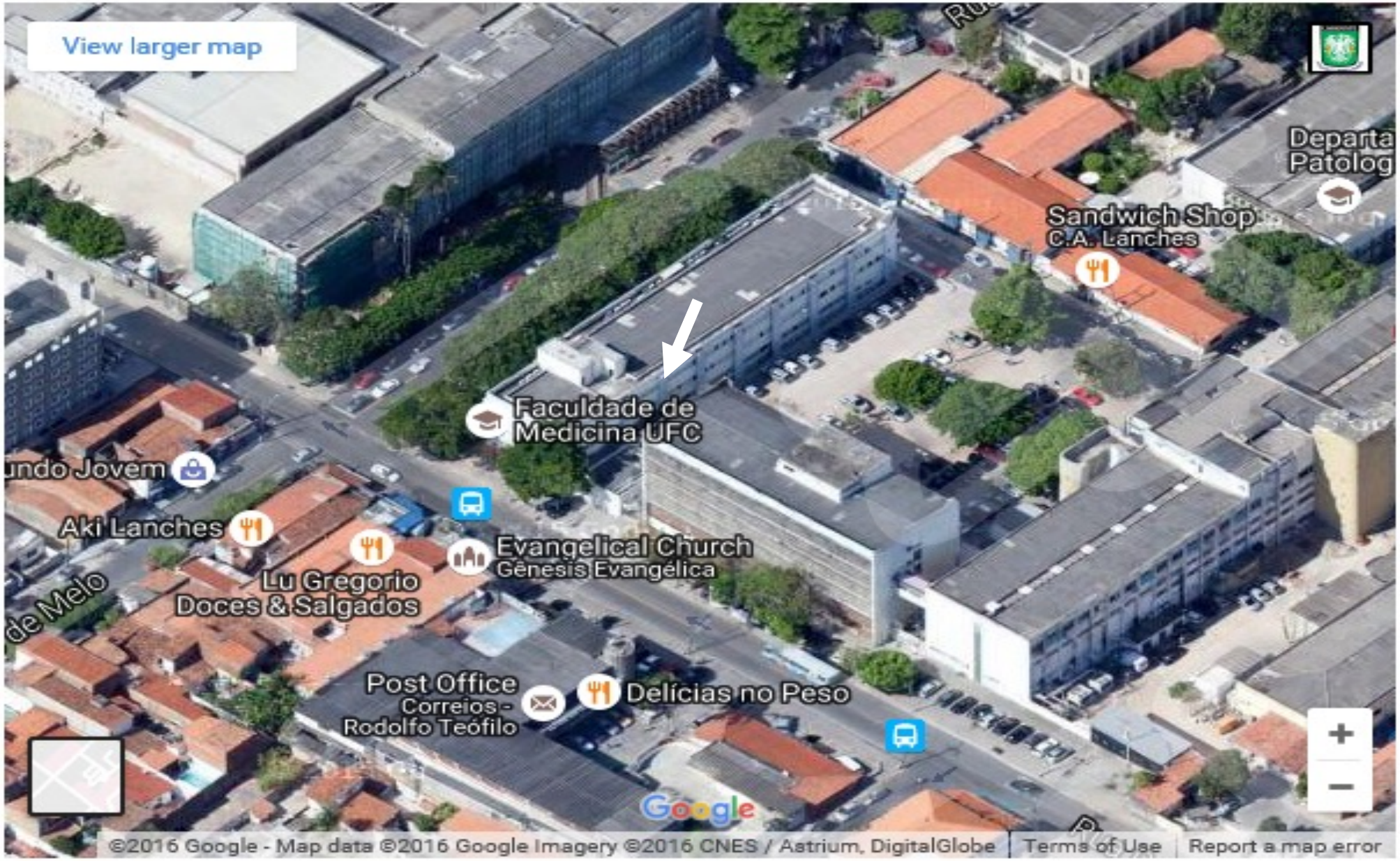

Nader, J et al, Nature Microbiology, 2019

Phylum: Apicomplexa
Genus: Cryptosporidium

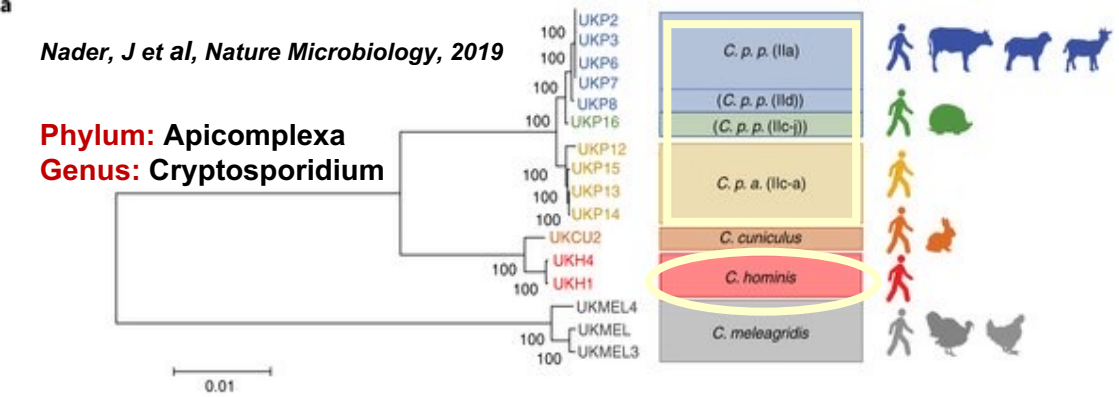

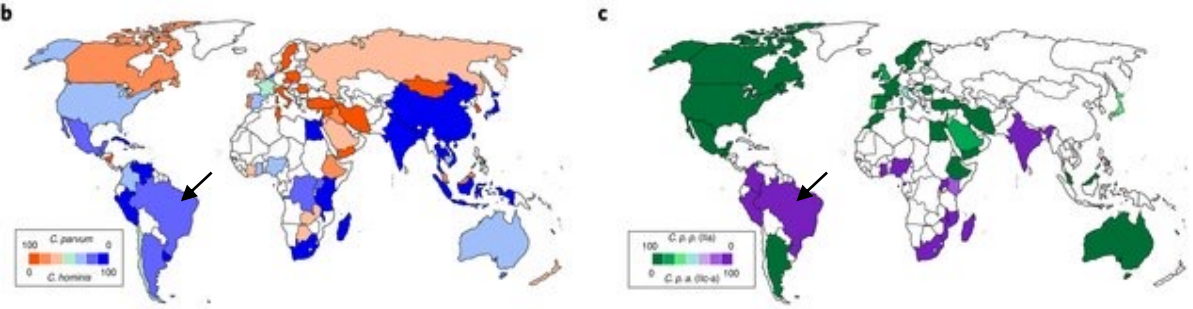

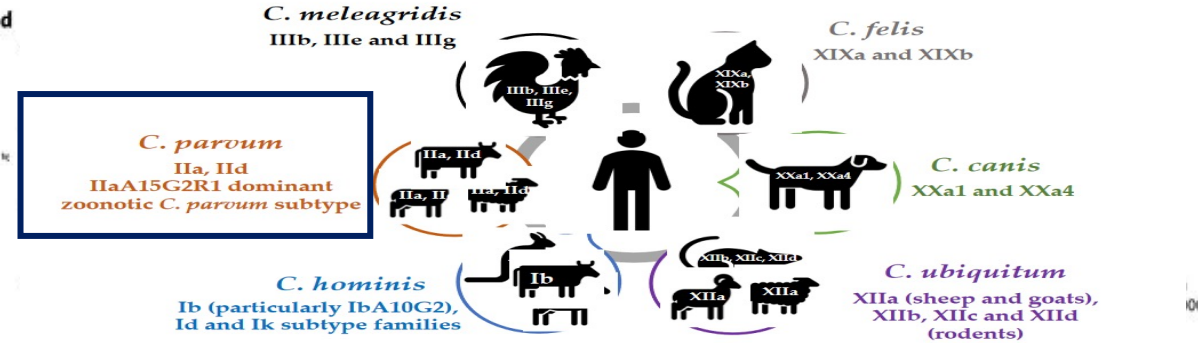

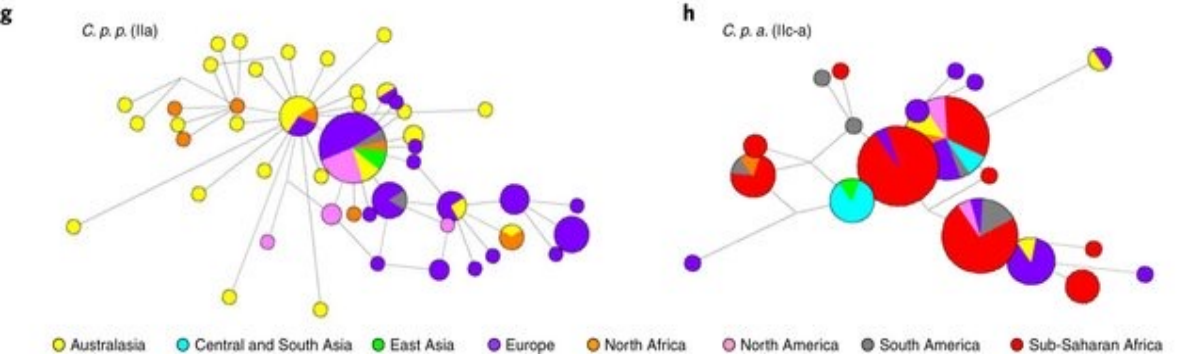

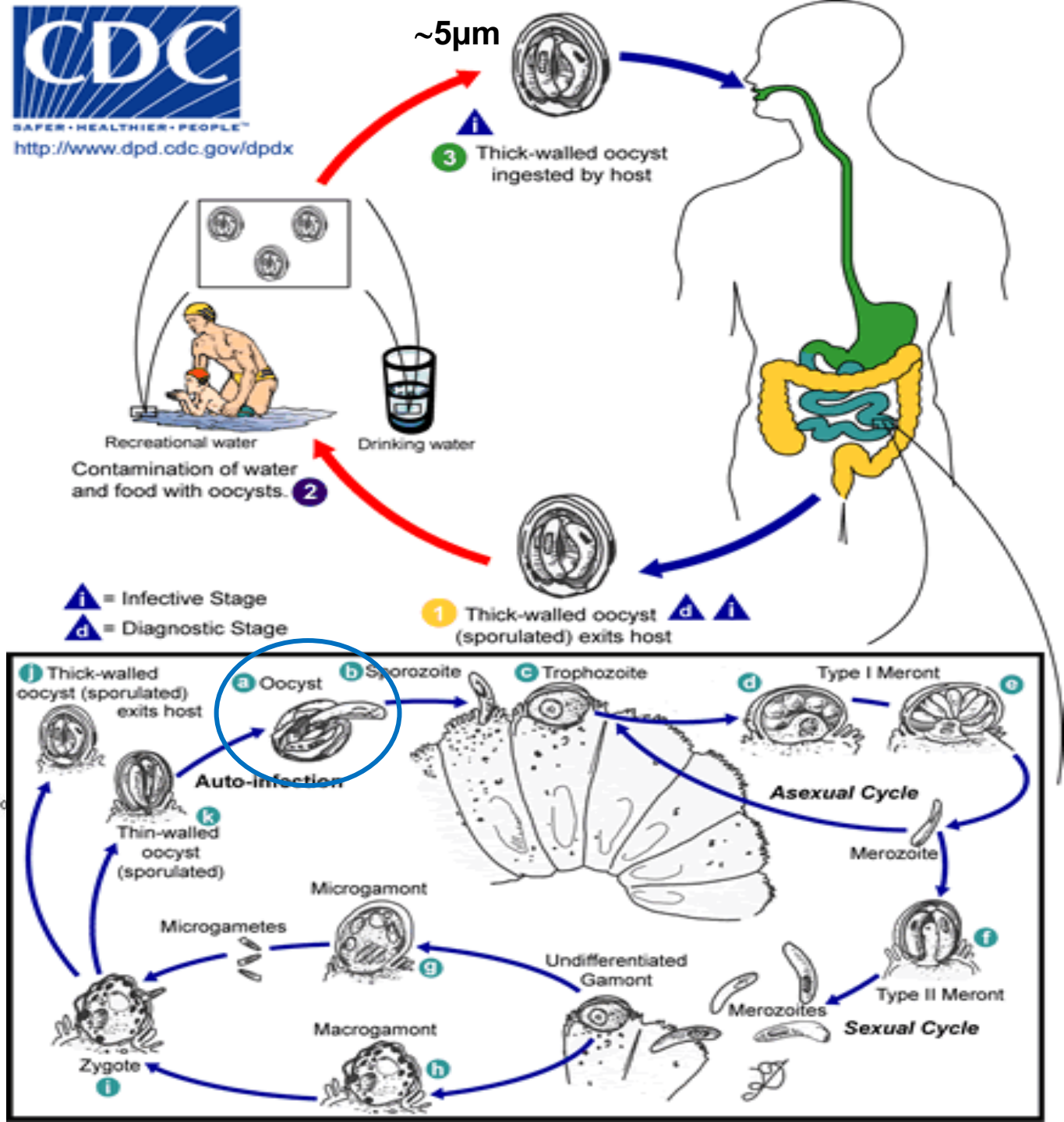

Cryptosporidium parvum cycle in humans and innate immune response

Stoyanova & Pavlov, Biom Rev, 2019

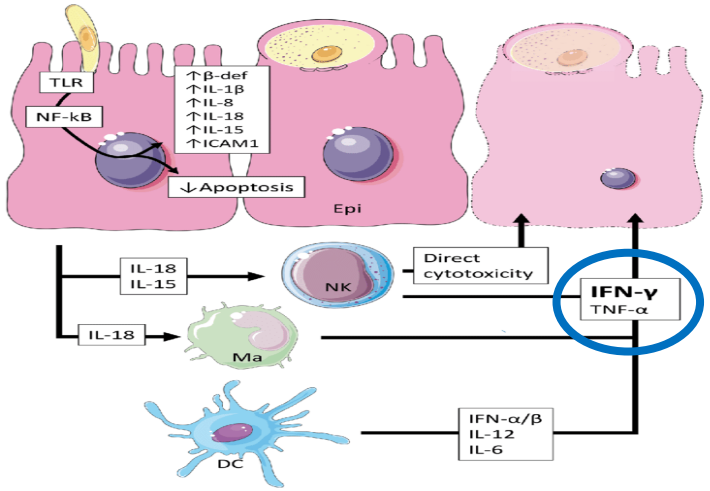

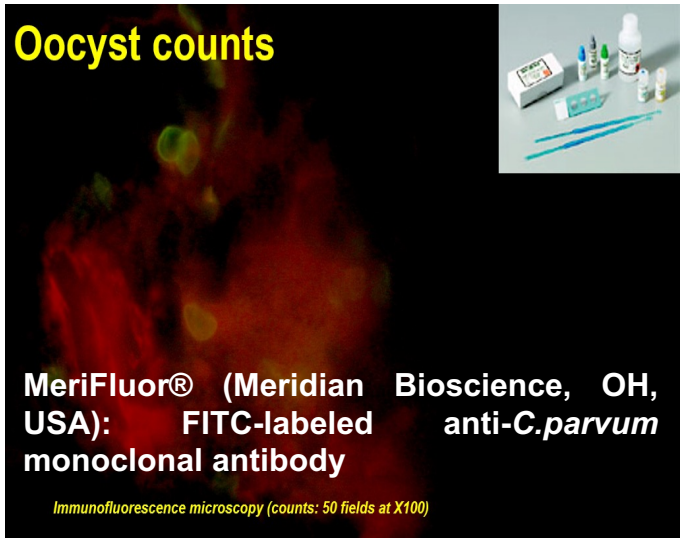

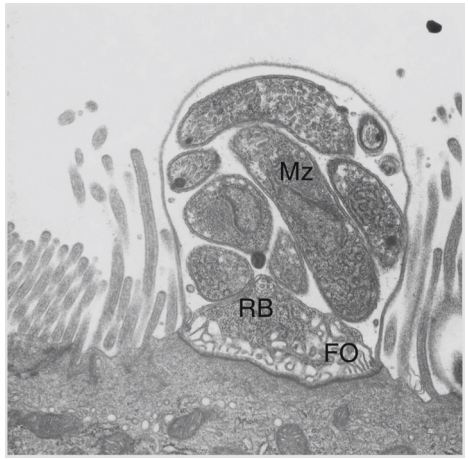

***C. parvum* type I meront in the jejunal epithelium**

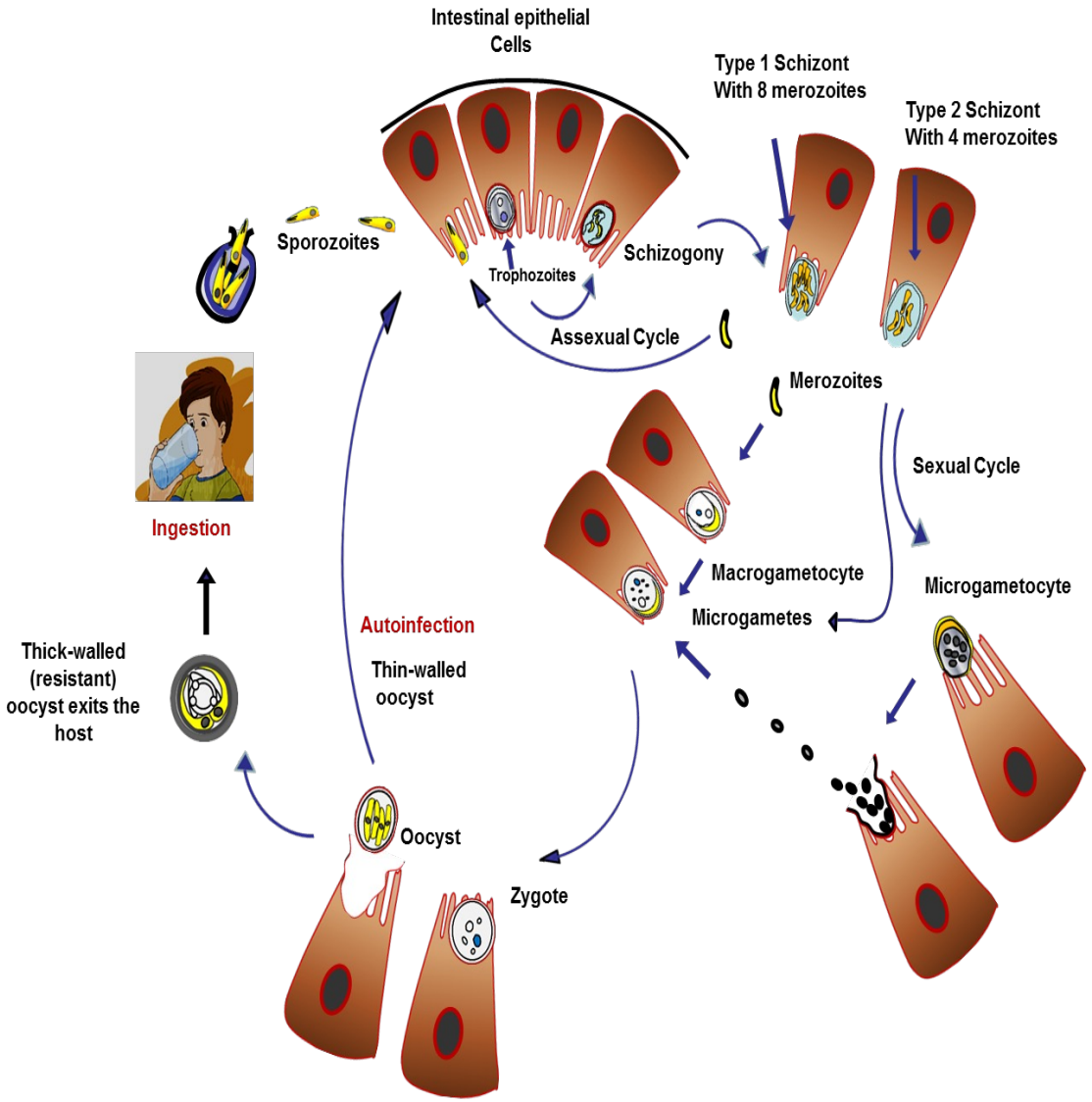

Oriá et al., 2017. Arginine and Its Use in Ameliorating *Cryptosporidium parvum* Infection in Undernourished Children. in: L-*Arginine in Clinical Nutrition*, Springer.

Cryptosporidium was found to be the second leading cause (5–15%) of moderate-to-severe diarrhea (MSD) in infants at all 7 GEMS study sites and third cause of MSD in toddlers age 12–23 months

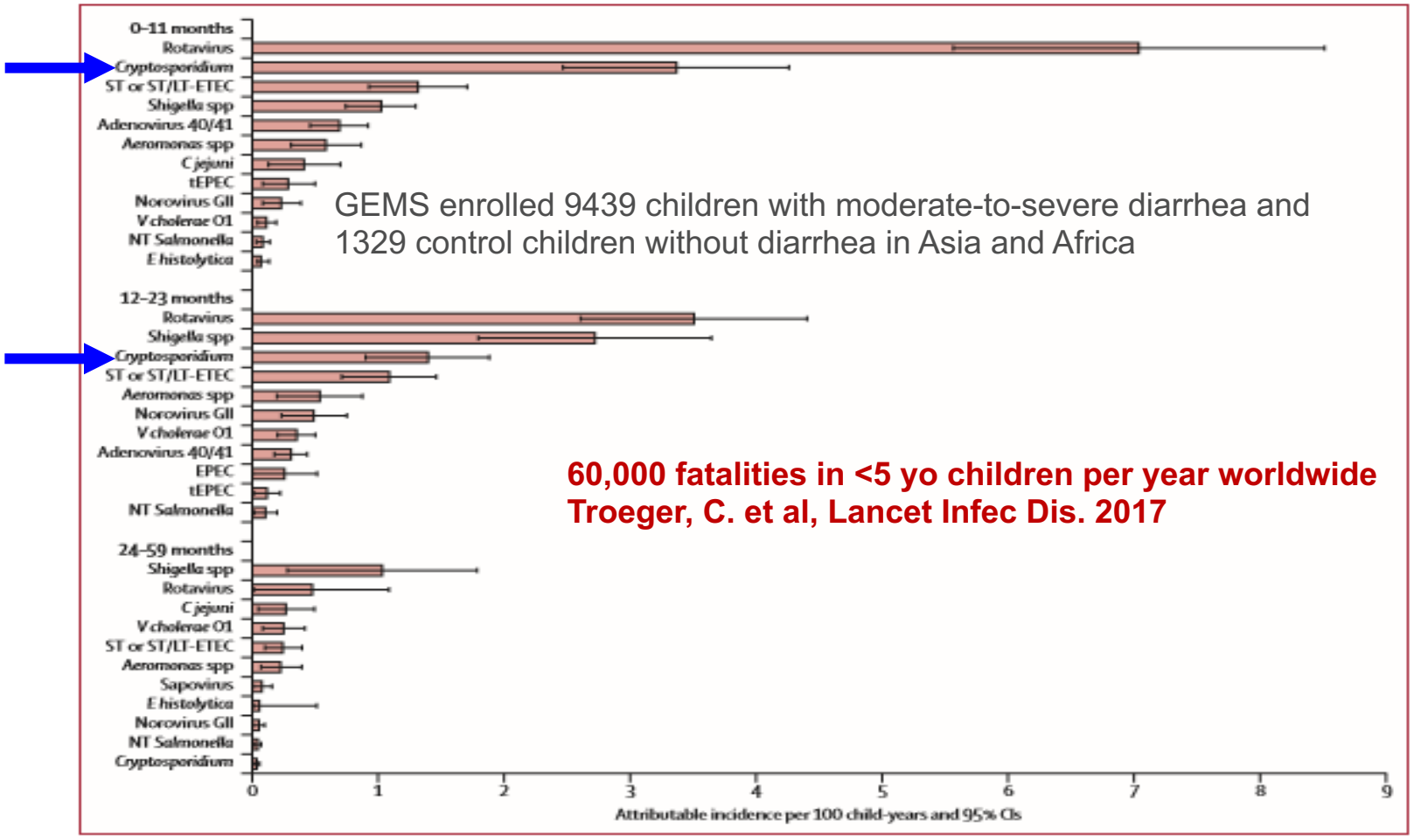

Kotloff, K.L et al, The Lancet, 2013, 382(9888):209-22

The Critical First 2 Years of Life for Brain And Gut:

Most (>75%) of Human Brain Growth & Synaptic Development

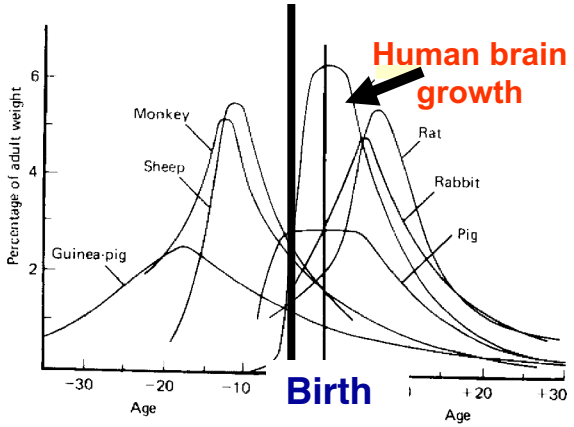

Human postnatal visual cortex

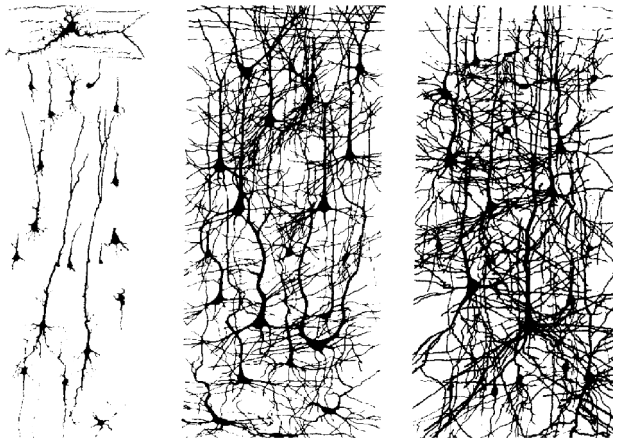

birth **15 mo** **2 yo**

Highest Rates of Diarrhea and Enteric Infections

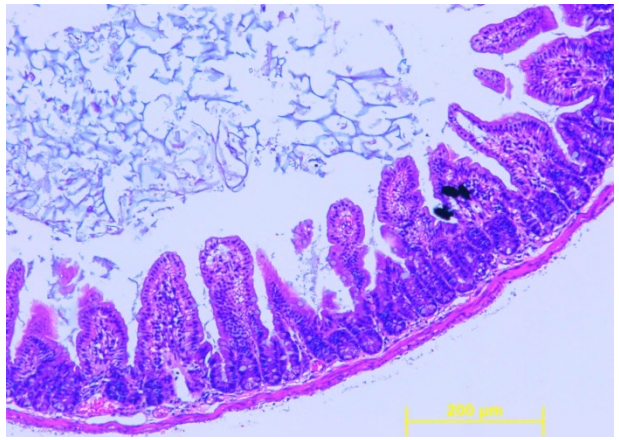

Normal **ileum**

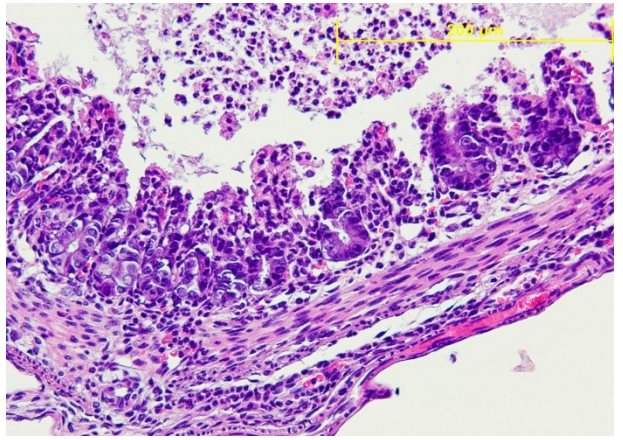

***Cryptosporidium*-infected**

+ only 1 opportunity for neuronal connections or 'forever lost'

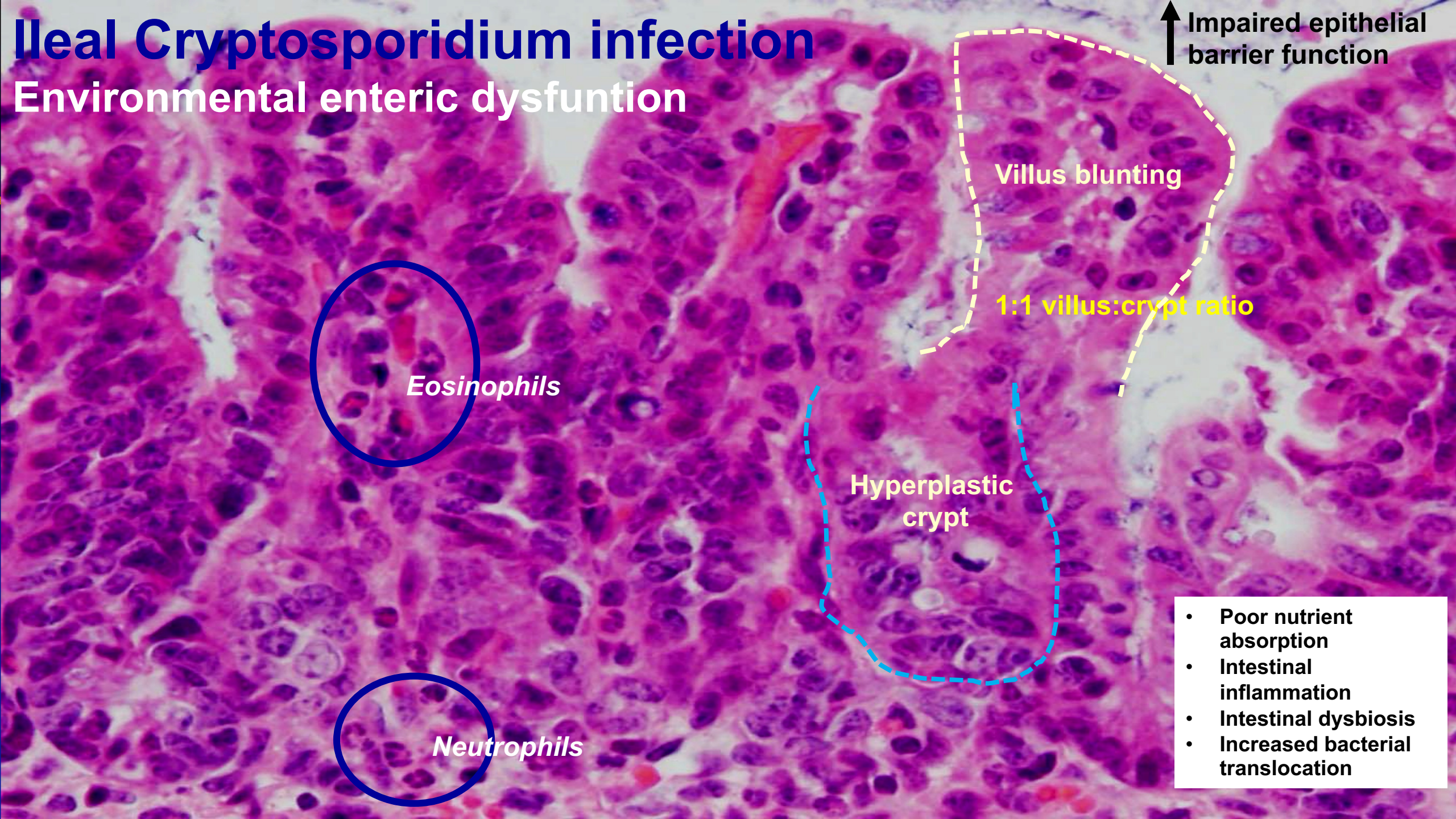
Ileal Cryptosporidium infection
Environmental enteric dysfuntion
Impaired epithelial barrier function
Villus blunting
1:1 villus:crypt ratio
Eosinophils
Hyperplastic crypt
Neutrophils
• Poor nutrient absorption
• Intestinal inflammation
• Intestinal dysbiosis
• Increased bacterial translocation

HYPOTHESIS

We hypothesize that systemic inflammation and/or EE biomarkers (intestinal barrier dysfunction and inflammation) due to *Cryptosporidium* infection and/or malnutrition will lead to meningeal macrophage and brain microglia activation with neuroinflammation.

Target brain region: prefrontal cortex

Prefrontal cortex development is critical for executive function

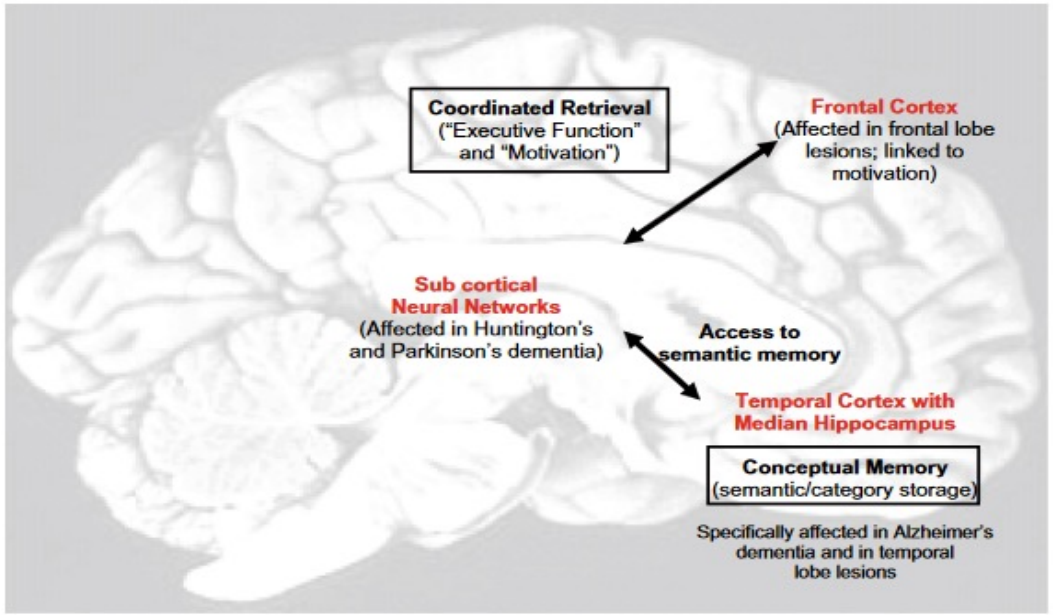

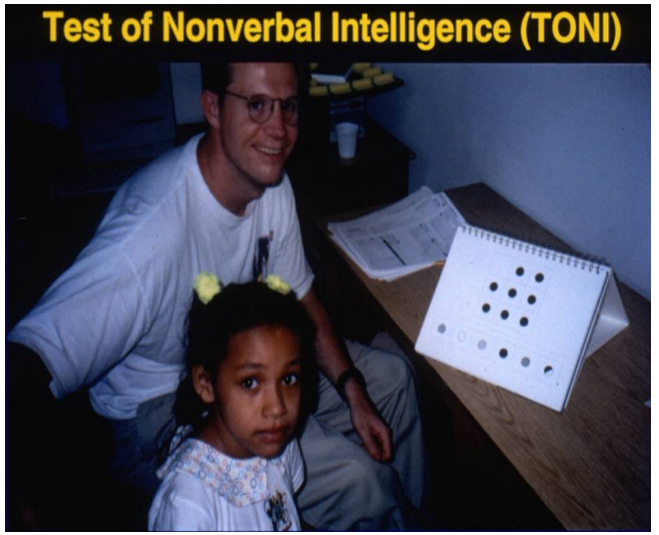

Function	Coordinated Retrieval ("Executive Function" and "Motivation")	Conceptual Memory (Long-term semantic category storage)
Site	Frontal Cortex Sub cortical Neural Networks	Temporal Cortex with Median Hippocampus
Main Diseases	Huntington's/Parkinson's diseases Frontal lobe or sub cortical lesions	Alzheimer's disease Temporal lobe lesions ***Early Childhood Diarrhea?***
Test(s)	Phonemic and semantic performance	Only semantic performance

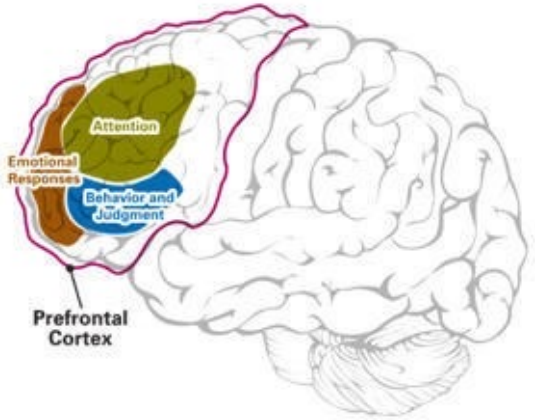

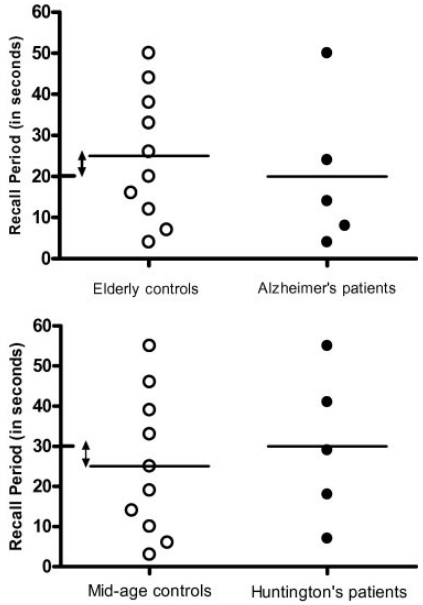

Oria et al, Medical Hypotheses, 2009

Environmental enteropathy biomarkers in children living in the northeast of Brazil

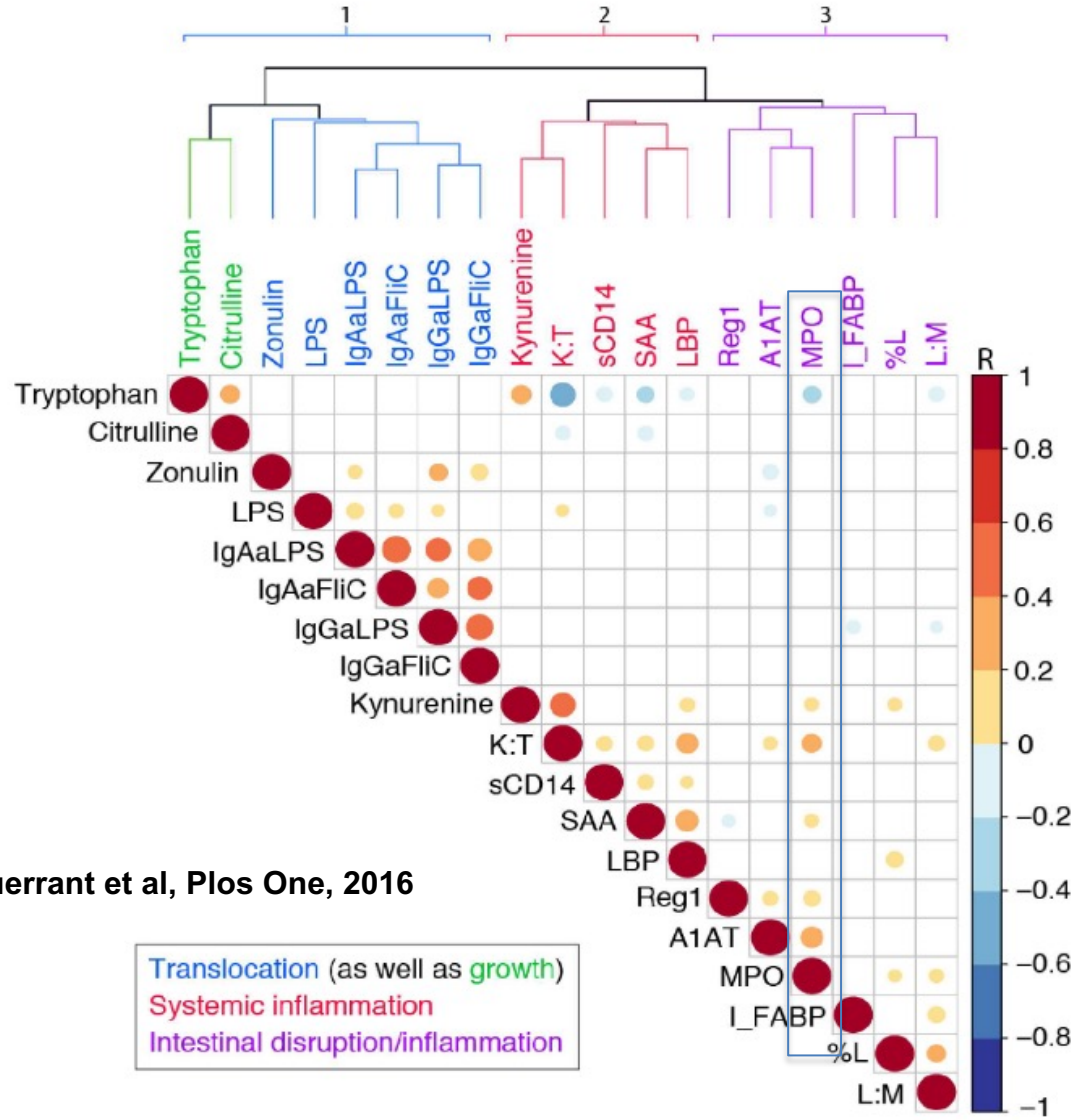

Guerrant et al, Plos One, 2016

Neutrophil-related granule content

Membrane proteins			
Azurophil granules	**Specific granules**	**Gelatinase granules**	**Secretory vesicles**
N.a.	CD11b/CD18, CD66, CD67	CD11b/CD18, CD67	CD11b/CD18, CD67
N.a.	Gp91phox/p22phox	Gp91phox/p22phox	Gp91phox/p22phox
N.a.		MMP25	MMP25
N.a.	TNFR[c], uPAR	TNFR[c]	LIR1–4,-6,-7,-9[c]; CD35; CD16; C1q-R; IFN-αR1 and IFN-αR2[c];IFN-γR1 and IFN-γR2[c]; TNFR1 and TNFR2[c]; IL-(1,4,6,10,13,17,18)R[c]; TGF-βR2[c]; CXCR-1[c]; CXCR-2[c]; CXCR-4[c]; CCR-1, -2, -3[c]; Ig(G,A,E)FcR[c]; TLR-1, -2, -4, -6, -8[c]; CD14; MyD88[c]; MD-2[c]; fMLPR; TREM1[c]
CD63, CD68, presenilin	SNAP-23, VAMP-2, Stomatin, PGLYRP[c]	SNAP-23, VAMP-2, Nramp1	SNAP-23, VAMP-2, Nramp1, alkaline phosphatase, DAF, CD10, CD13
Matrix Proteins			
Elastase, cathepsin G, proteinase 3	Collagenase, Gelatinase, uPA, cystatin C[c], cystatin F[c]	Gelatinase, arginase 1	Plasma proteins
Defensins, BPI, MPO, lysozyme	hCAP18, NGAL, B12BP, lysozyme, lactoferrin, haptoglobin, pentraxin 3, prodefensin	Lysozyme	N.a.
Sialidase, Azurocidin, β-glucoronidase, azurocidin	α1-anti-trypsin[c], SLPI, orosomucoid, heparanase, β2-microglobulin, CRISP3	β2-microglobulin, CRISP3	N.a.

Borregaard et al, Trends in Immunology, 2007

Aims and Methods summary:

Evaluate the gut-brain axis, with a focus on environmental enteropathy markers leading to meningeal and brain inflammation following crypto infection and malnutrition

EE BIOMARKERS:
Intestinal inflammation: Cecal MPO and fecal lipocalin-2

SYSTEMIC INFLAMMATION:
Serum Amyloid A (SAA)

PARASITE BURDEN
Stool *C. parvum* oocyst shedding

BRAIN/MENINGEAL IMMUNOLOGY:
Meninge flow cytometry
NF-κb, MPO, and cytokines expression.

GROWTH MARKERS
Weight, body and tail length curves

No studies have addressed Crypto infection effects in the brain and meninges before.

Methods

- **Monitoring: growth curves (weight gain and tail length), parasite stool shedding, and stool inflammatory markers.**
- **Blood samples for serum amyloid A (SAA), as biomarker of systemic inflammation.**

After euthanasia (euthanasia: days 14th, on day 6 post-inf)

Flow cytometry of meningeal cell suspension

NOS2 immunohistochemistry for meninges

PFC IBA-1 immunostaining

Luminex assay for brain cytokines

Cecal and PFC myeloperoxidase (MPO) content analyses

Methodology/design

- 3-week-old C57BL/6 mice
- Diets for 2 weeks:
  - dND (defined nourished diet)
  - dPD (protein deficient diet)

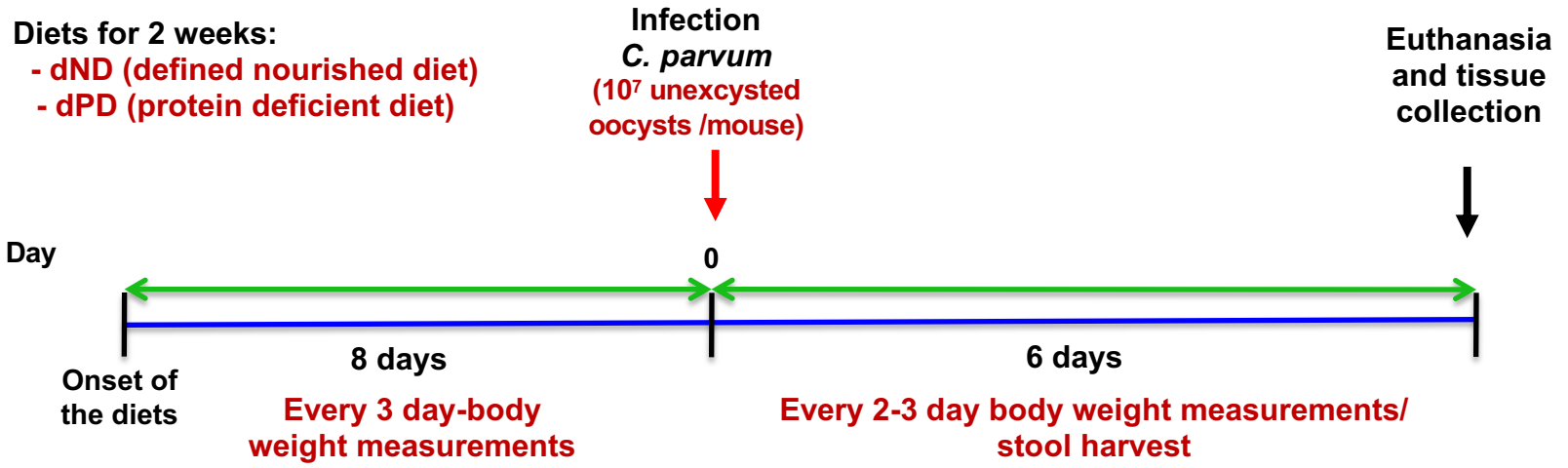

After infection, stools were assessed for *C. parvum* oocyst shedding and inflammatory biomarkers. Mouse tail and body length were measured at the endpoint.

Undernourished mice challenged with a defined protein deficient diet (dPD) for 8 days showed impaired weight gain.

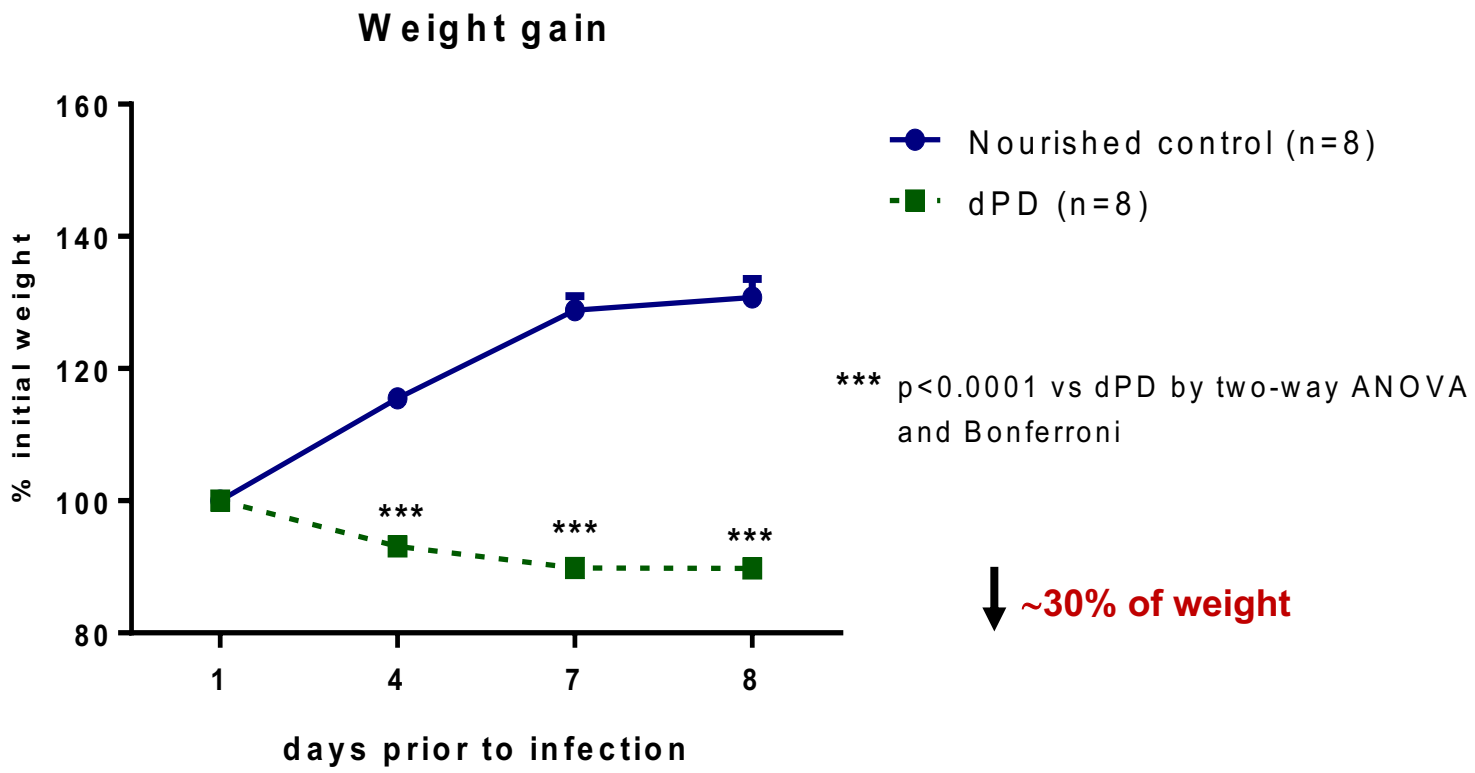

Undernourished mice challenged with a defined protein deficient diet (dPD) for 8 days showed higher stool lipocalin-2 levels

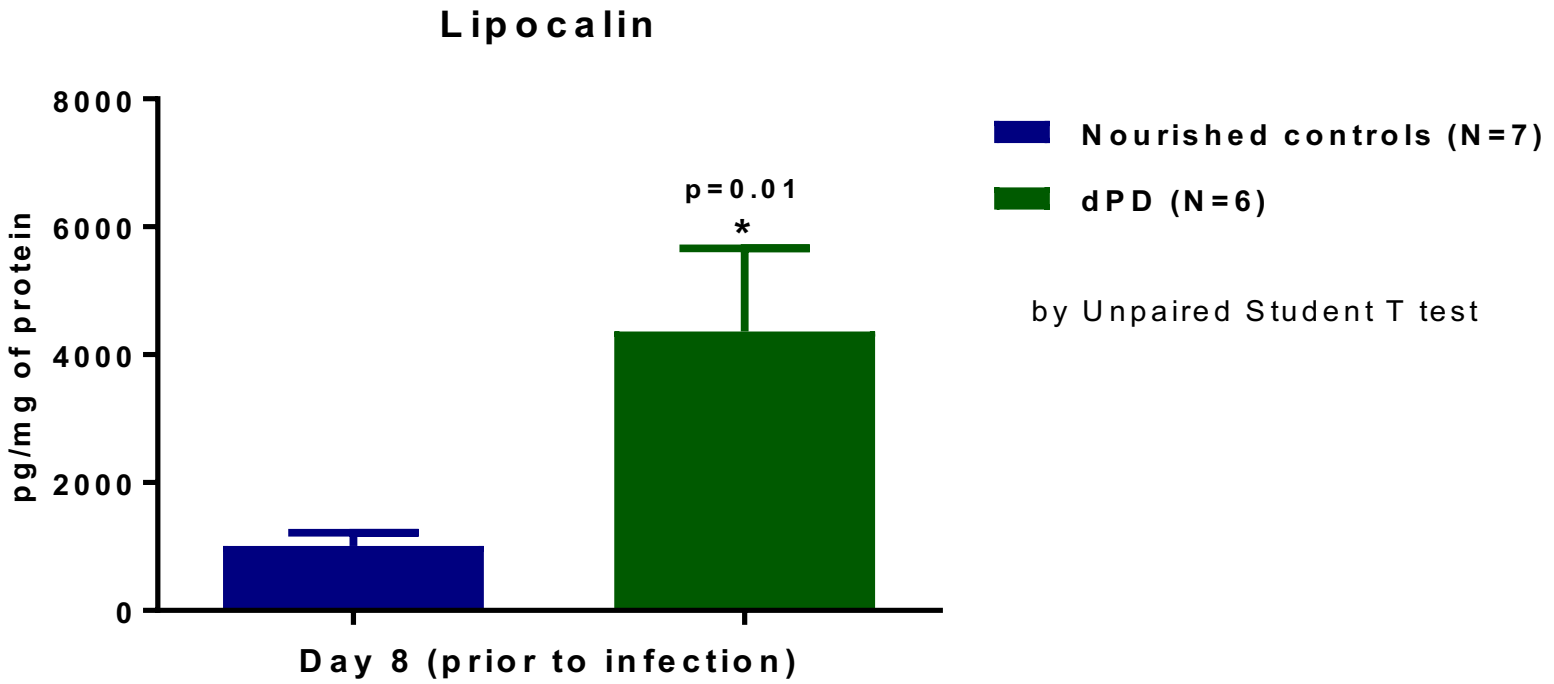

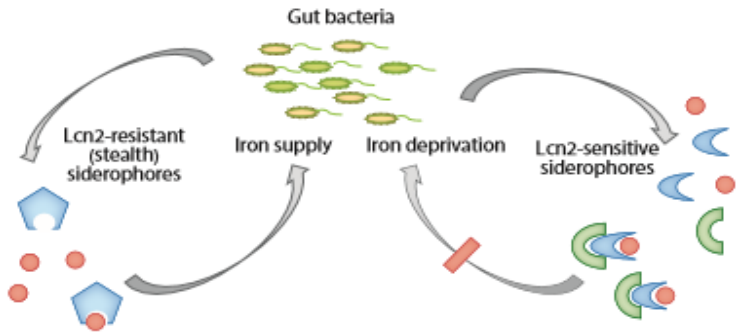

LCN/NGAL reduces iron availability to bacteria!

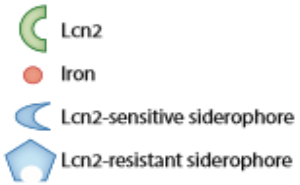

Xiao, X. et al, Annual Review of Nutrition, 2017

Undernourished C. parvum infected mice showed significantly lower weight gain as compared with uninfected controls.

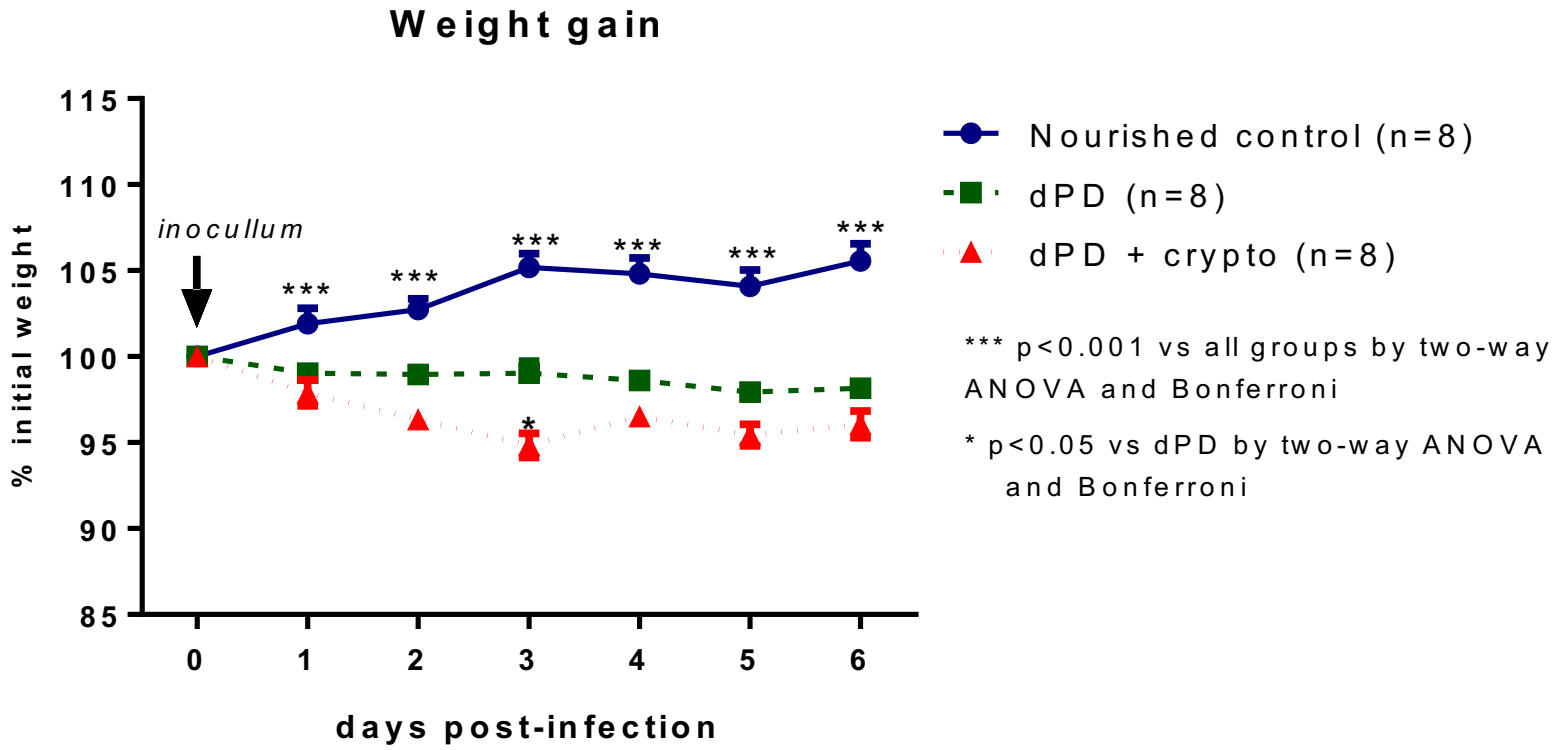

Undernourished mice were infected by an innoculum of 2 X 10^7 unexcysted C. parvum occysts by gavage.
Nourished controls were not infected.

Real-time qPCR with 10^{2-7} Crypto. oocysts in fecal samples

(using 18S rRNA primers; showing quantification in stool to test *in vivo* infection)

CT values of each run were compared to standards with known amount of *C. parvum* DNA and log transformed. Results are shown as the number of oocysts per 100 mg of stool sample

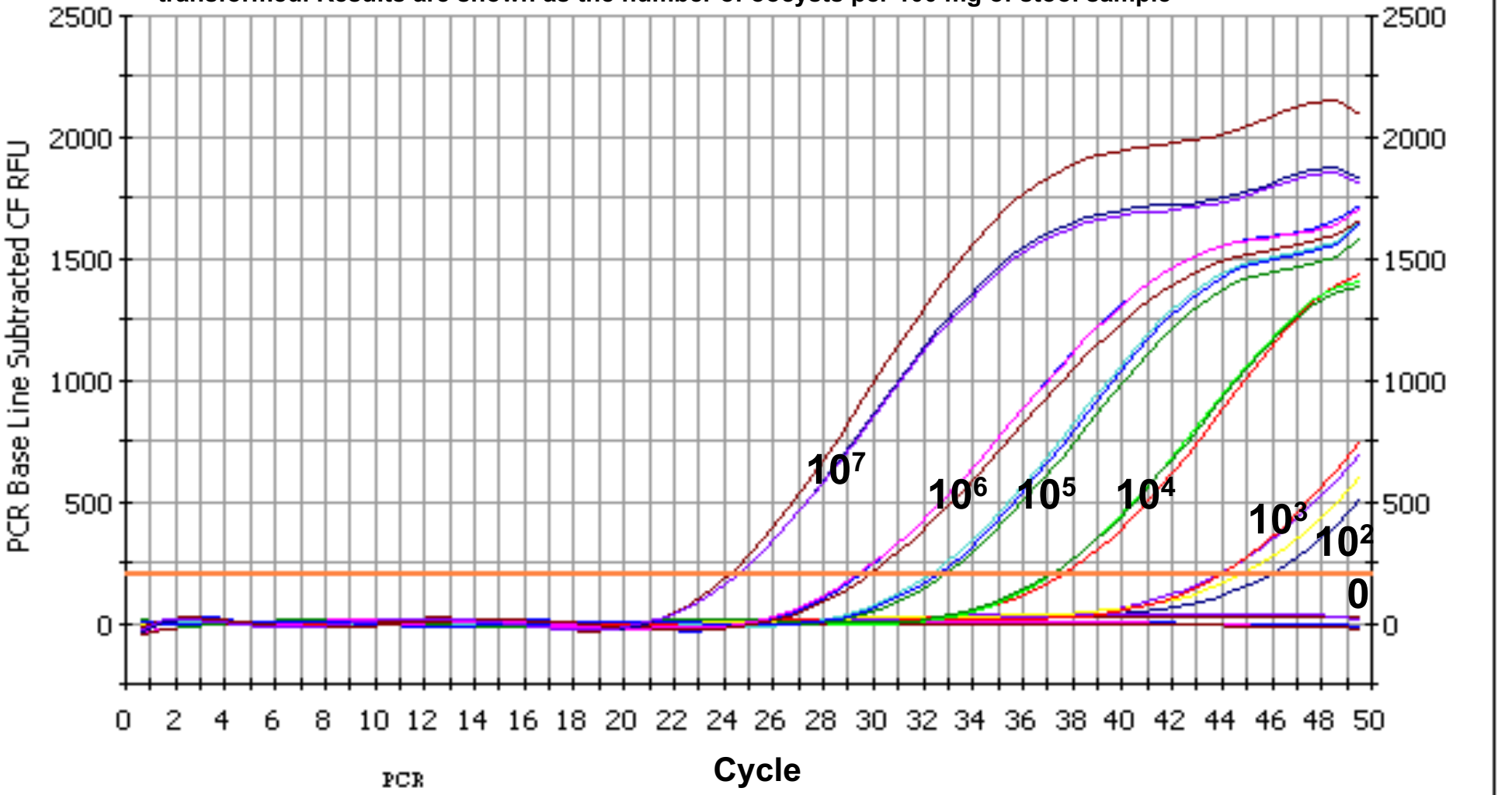

Parr, Sevilleja, Vieira, Oria et al. 2005.

Undernourished C. parvum infected mice showed sustained stool oocyst shedding following infection

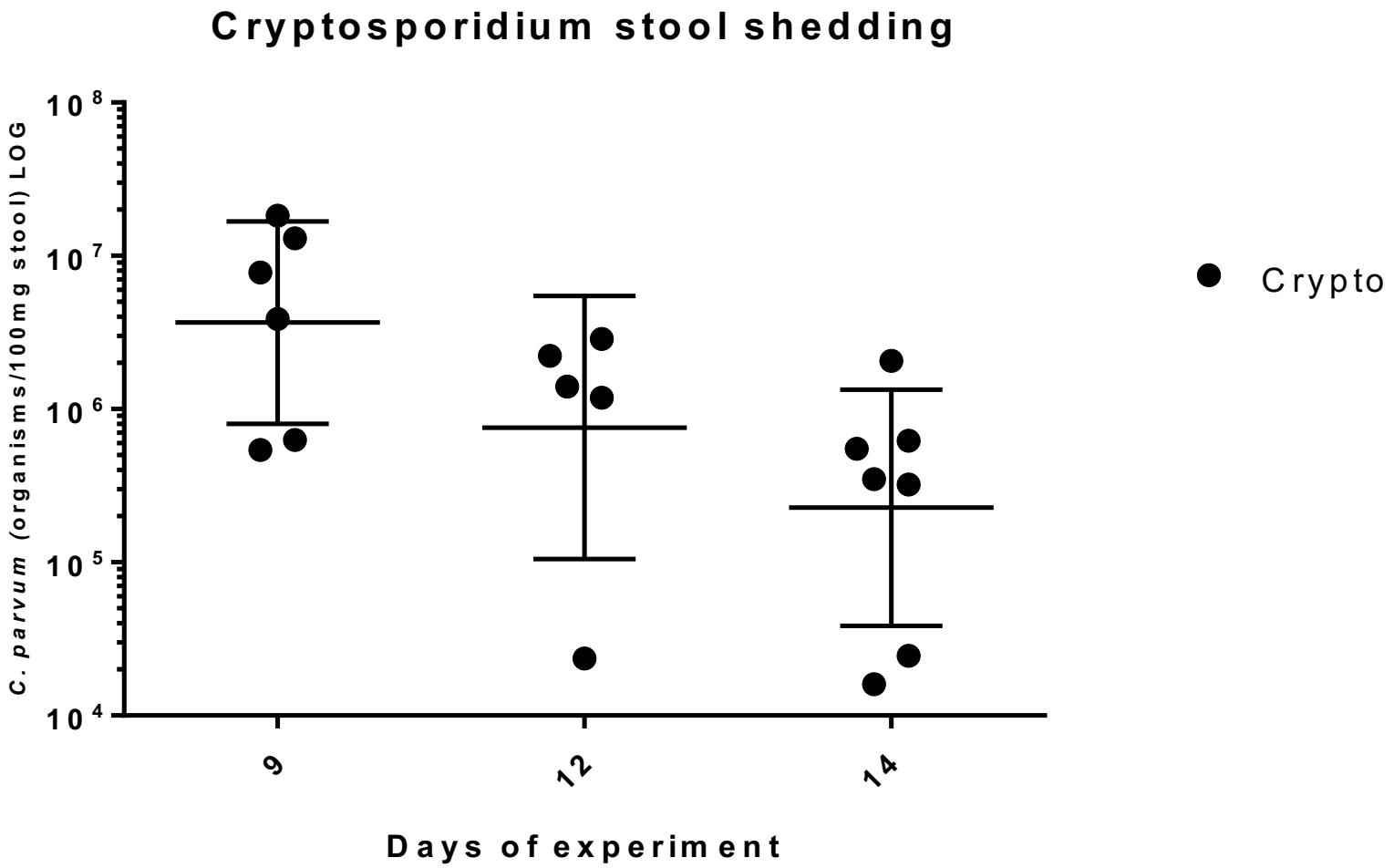

The primers target the 18 s rRNA gene of the parasite in the stools by RT-PCR

Undernourished C. parvum infected mice showed significantly lower tail and body length as compared with uninfected controls.

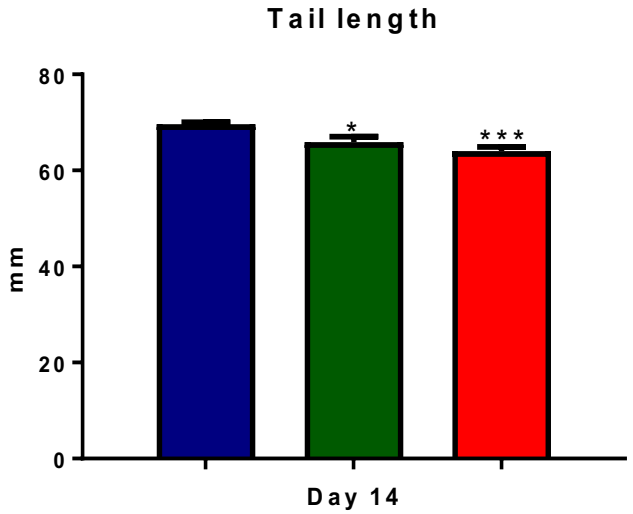

Nourished control (n=8)
PD (n=8)
PD + Crypto (n=8)

*p<0.05 by one-way ANOVA vs
vs nourished control

***p<0.001 by one-way ANOVA vs
vs nourished control

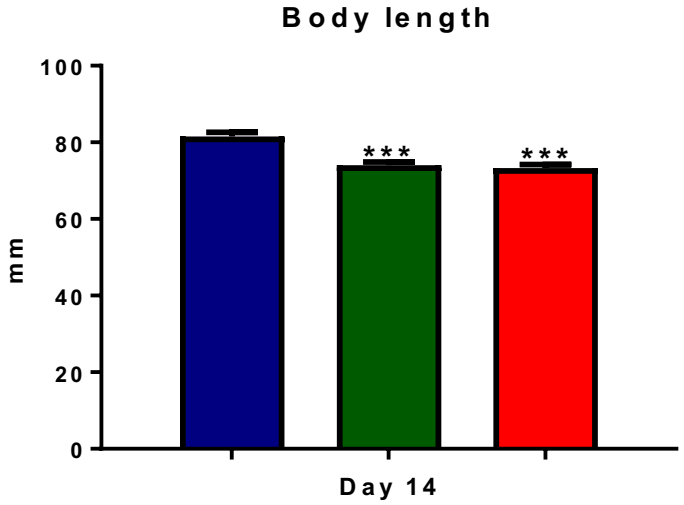

Nourished control (n=8)
PD (n=8)
PD + Crypto (n=8)

p<0.001 vs nourished control, by
*one-way ANOVA and Bonferroni

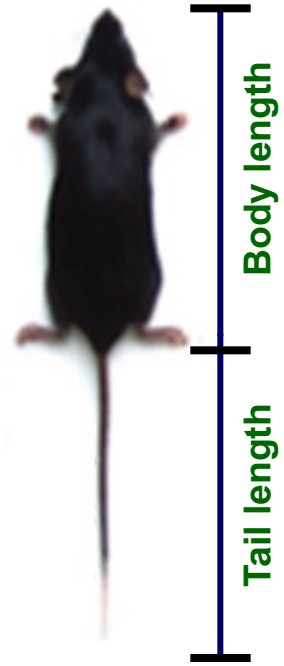

Representative ileal H&E histology from uninfected (nourished or dPD) and infected mice (dPD + Crypto) at day 7 post-infection. *C. parvum* induces ileal mucosal disruption

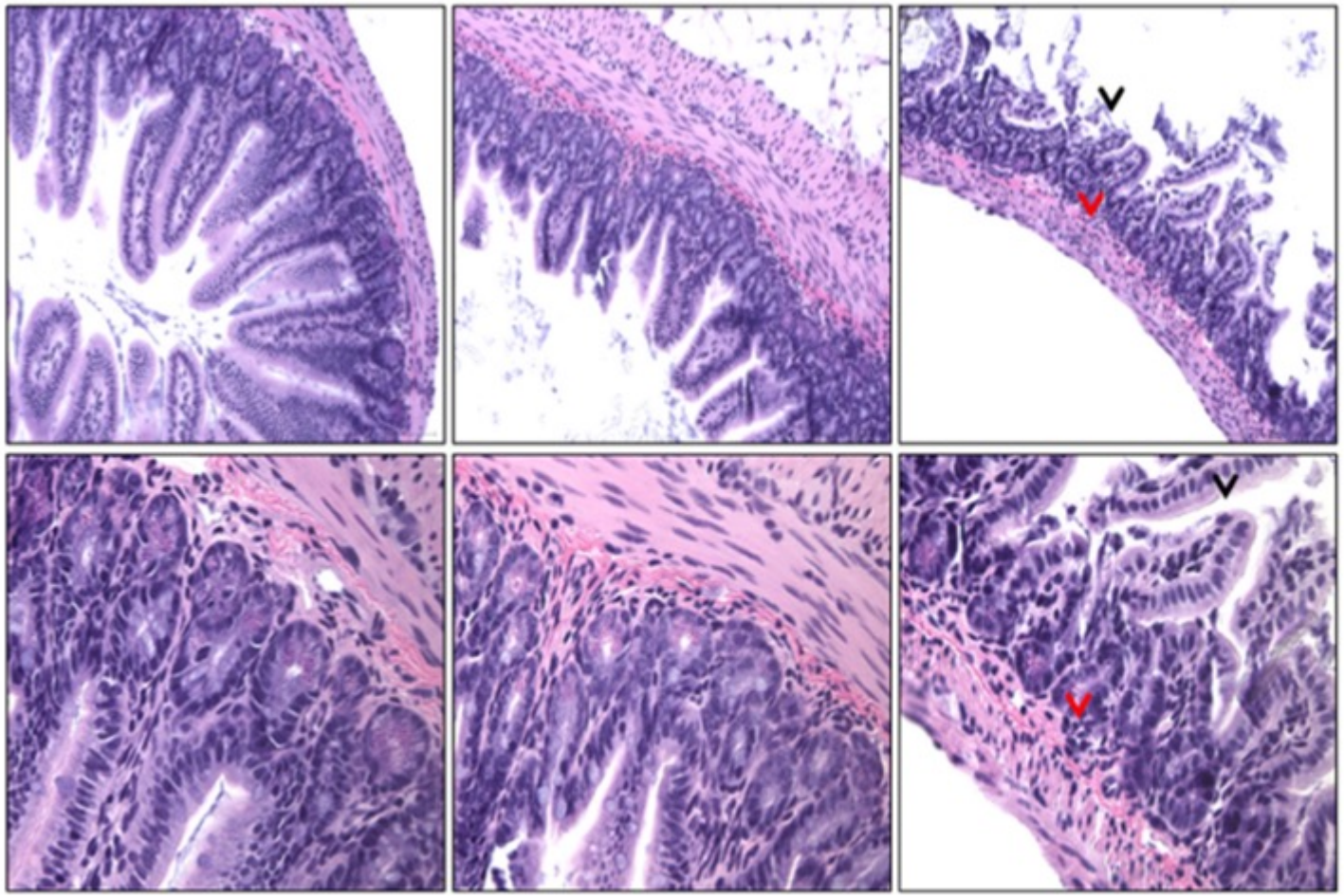

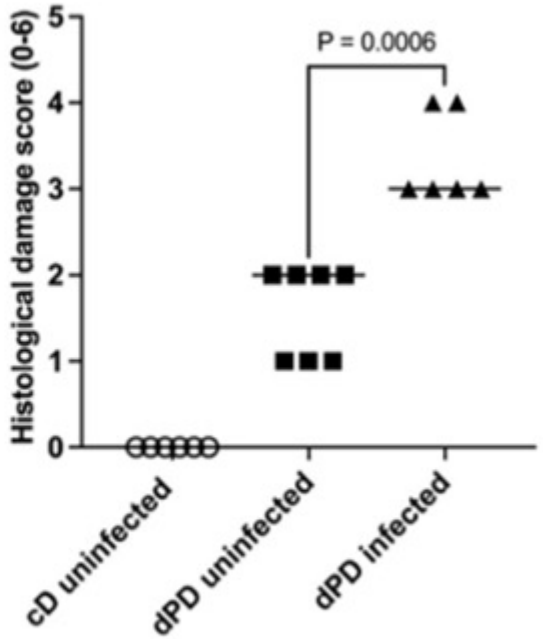

Histopathology Damage Score (sum of epithelial and cell infiltration scores): 0=no damage; 1= mild; 2=moderate, 3=extensive. Max. Damage Score=6)

Undernourished C. parvum infected mice showed significantly higher fecal lipocalin-2 (LCN-2) compared with uninfected controls.

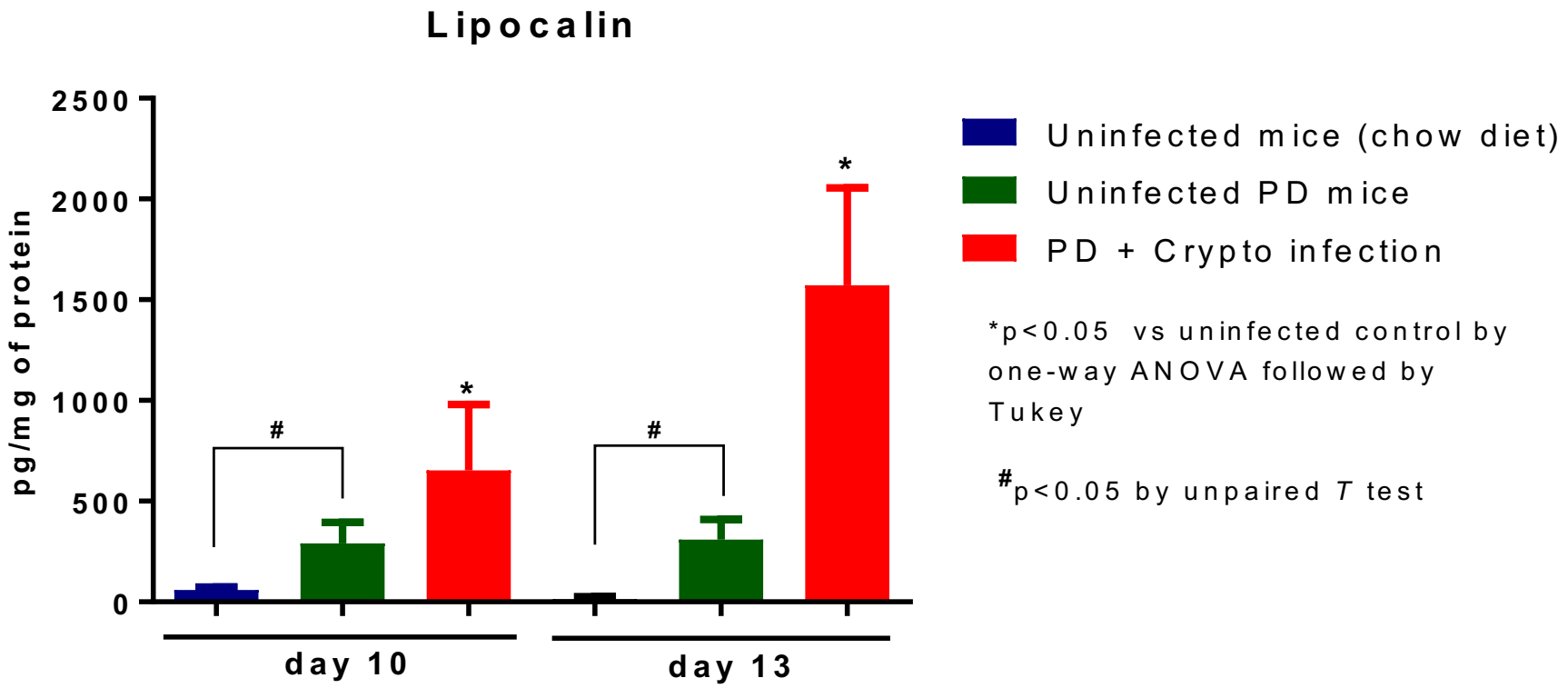

Undernourished C. parvum infected mice showed significantly higher cecal MPO on day 14 (6 days post-infection)

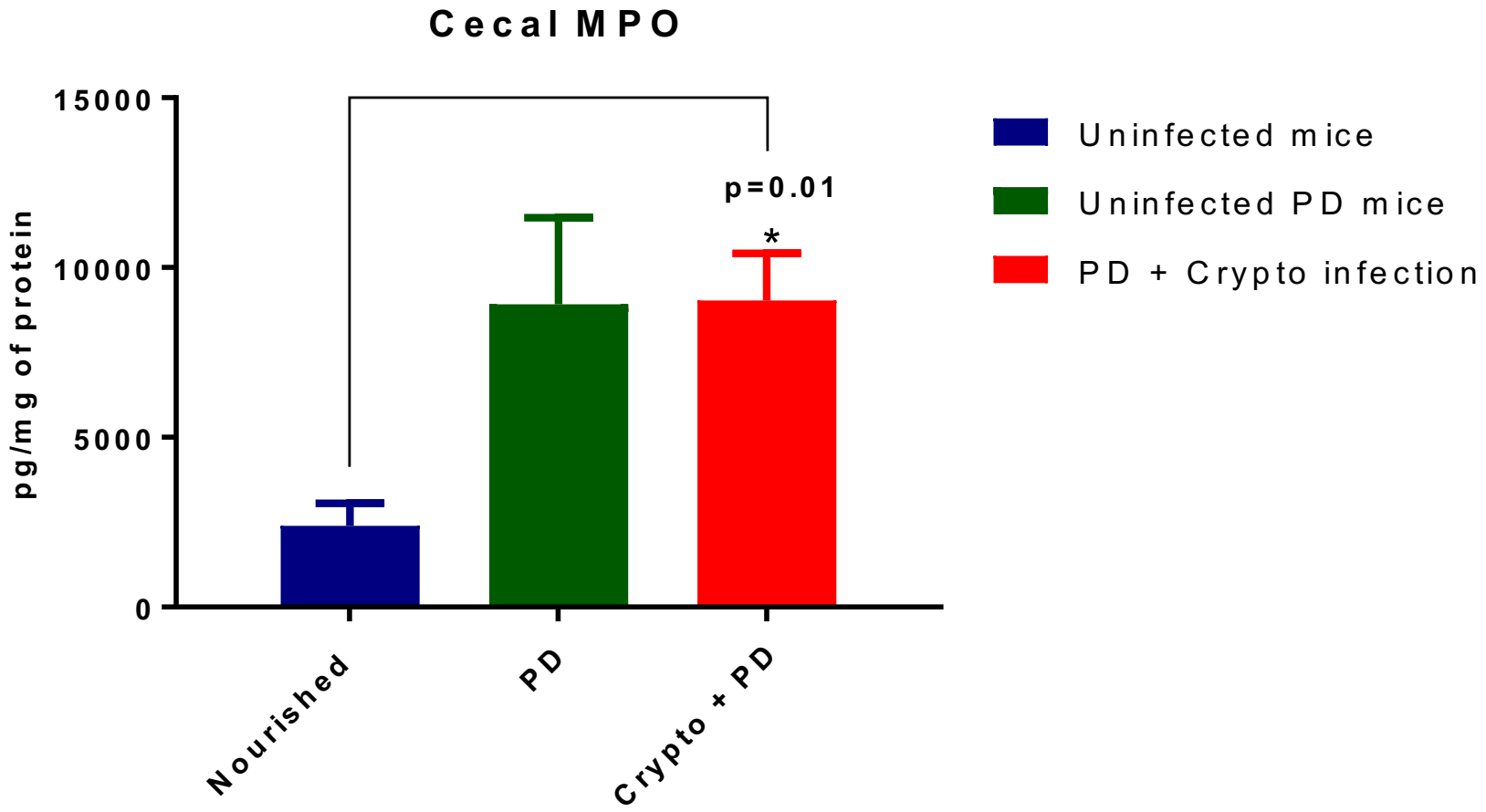

Myeloperoxidase (MPO) is a marker of tissue neutrophil infiltration and inflammation. MPO is found in the azurofilic granules from neutrophils.

Serum amyloid A (SAA) is significantly higher after dPD and Crypto infection compared with uninfected nourished controls

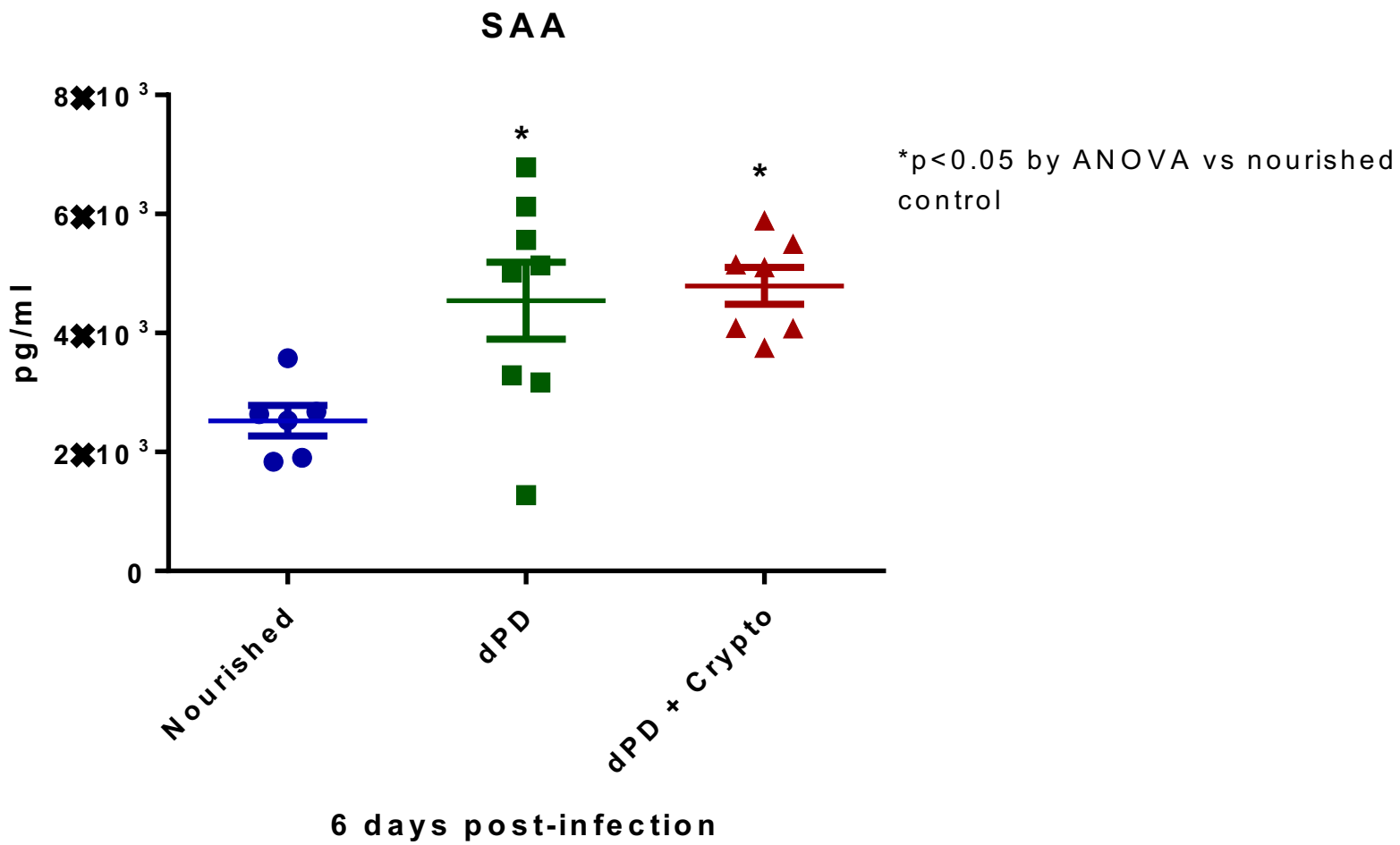

Serum amyloid A (SAA), a marker of systemic inflammation, may affect LPS neutralization.

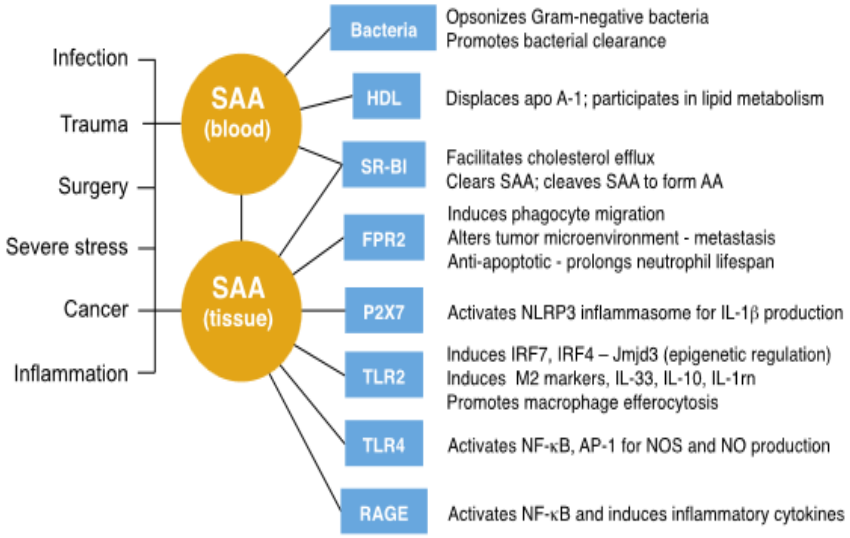

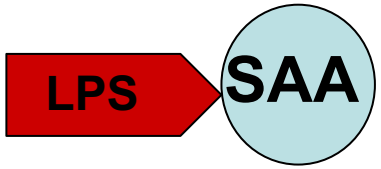

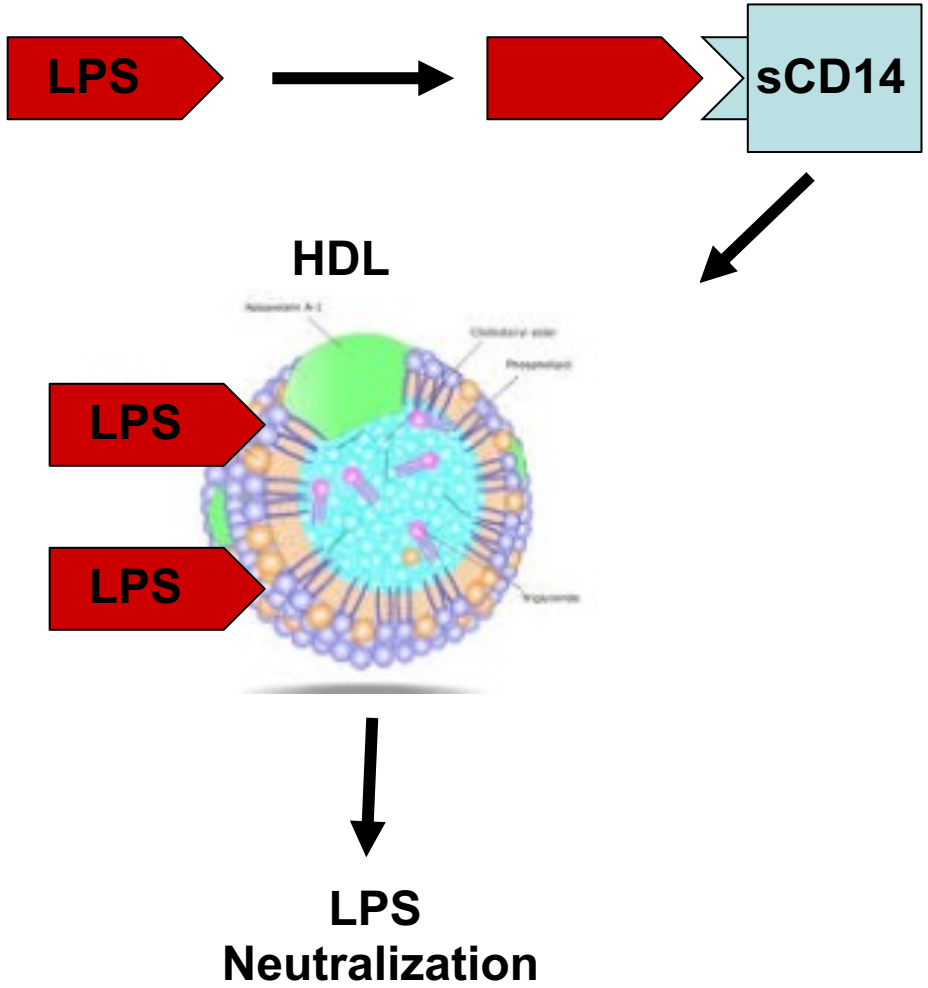

Adapted from Wu, A. et al, Shock, 2004
Ye, RD, Sun L. J. Leuk. Biol, 2015

Brain meningeal cell population in homeostasis

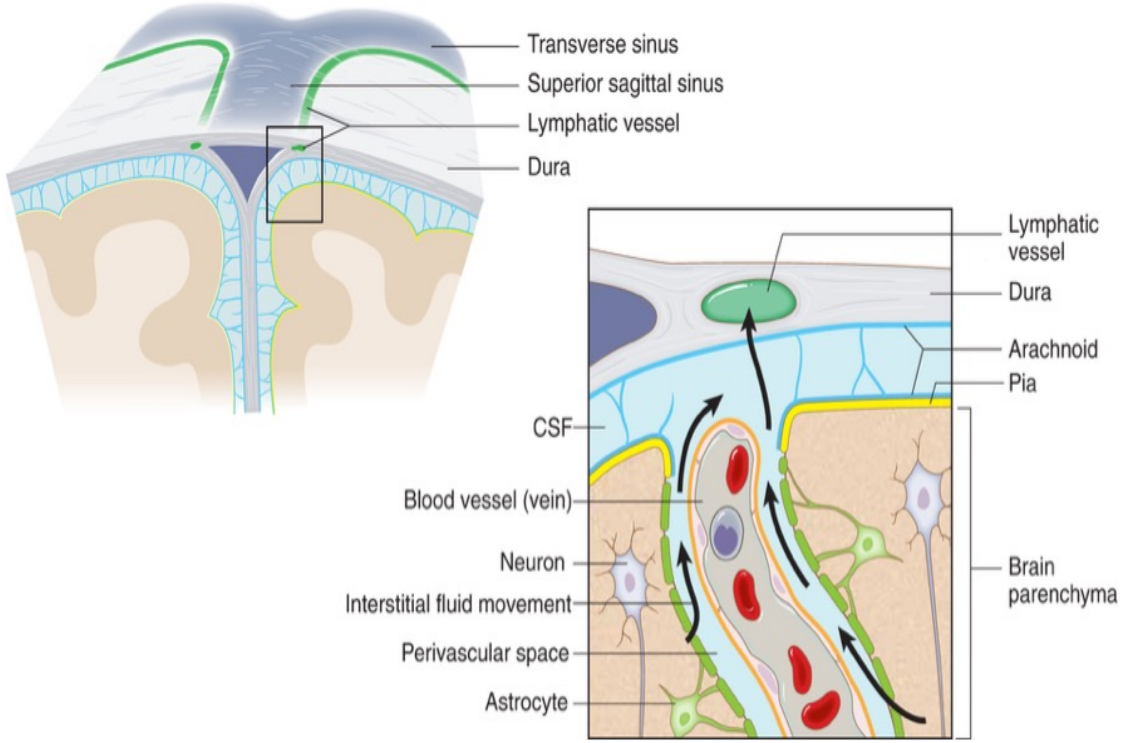

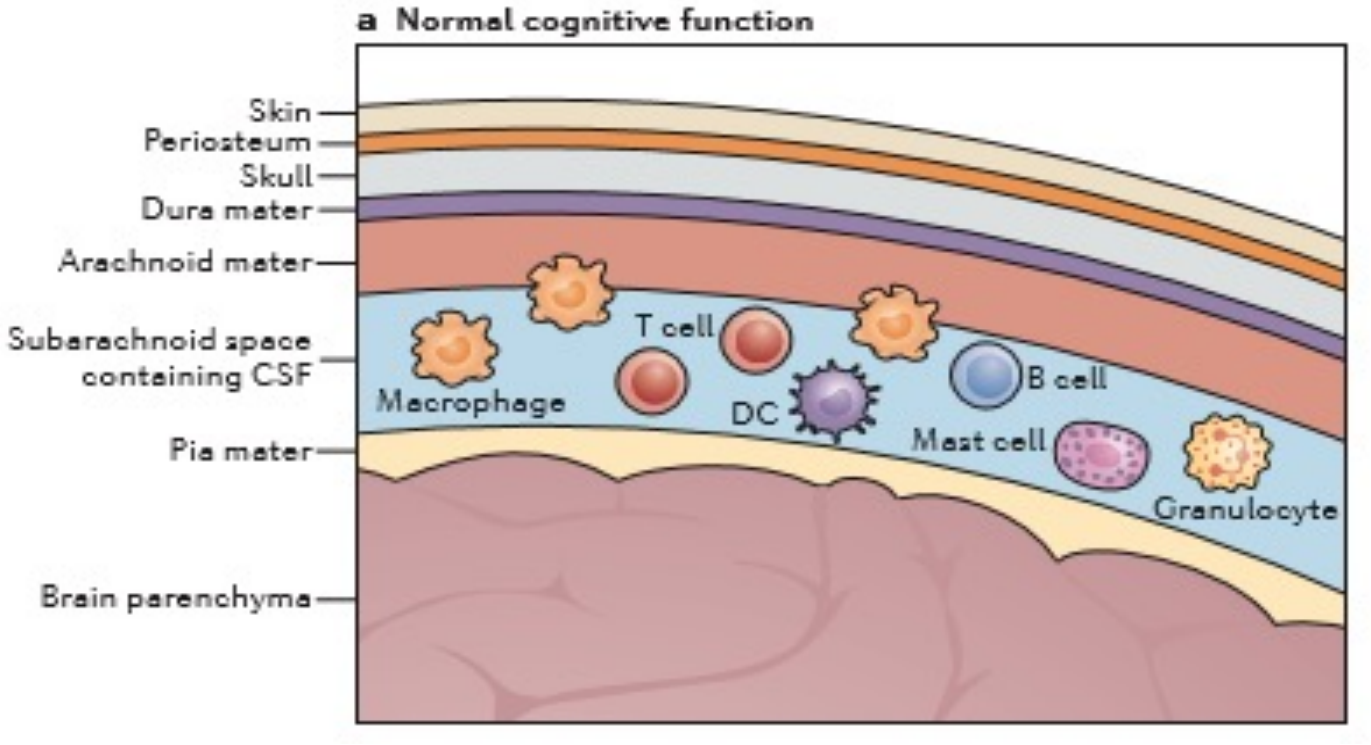

Kipnis, J. et al, Nature Reviews Immunology, 2012

Would changes in the meningeal B or T cell compartment increase the risk of brain inflammation?

Flow cytometry analyses of meningeal cell suspension following C. parvum infection and controls (6 days post-infection)

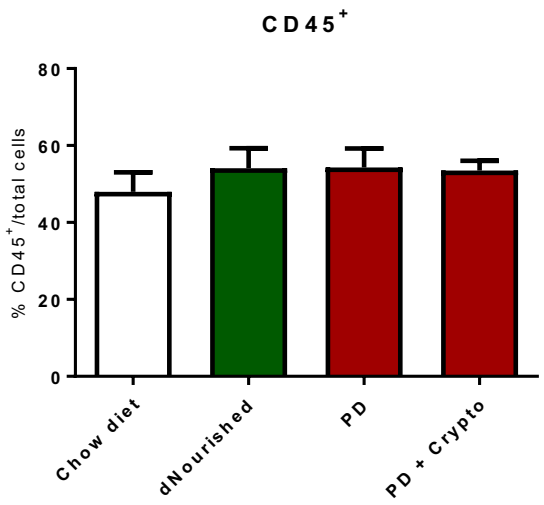

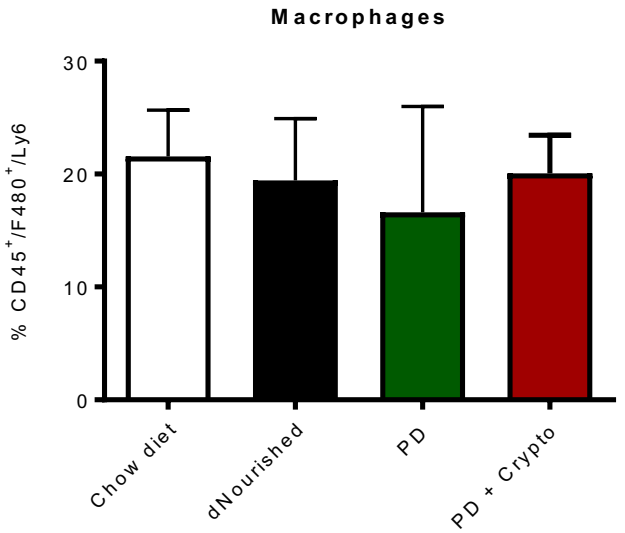

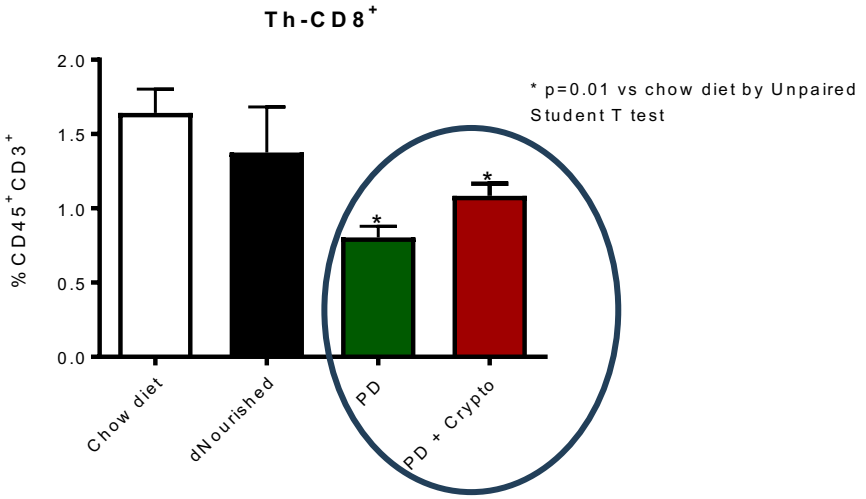

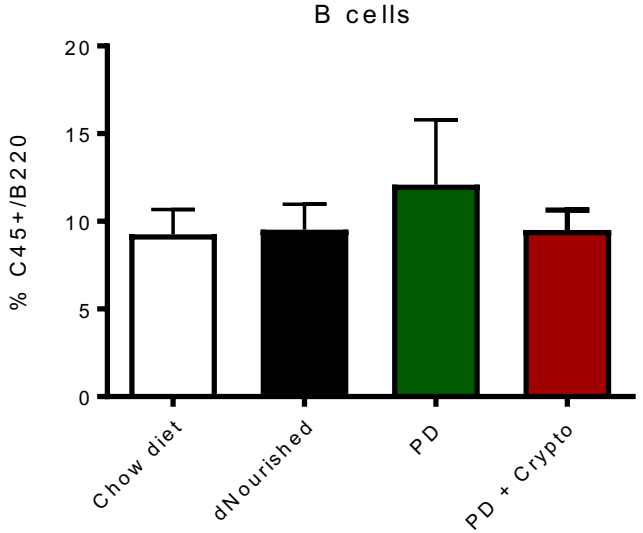

Flow cytometry gating strategy for T-cell analysis

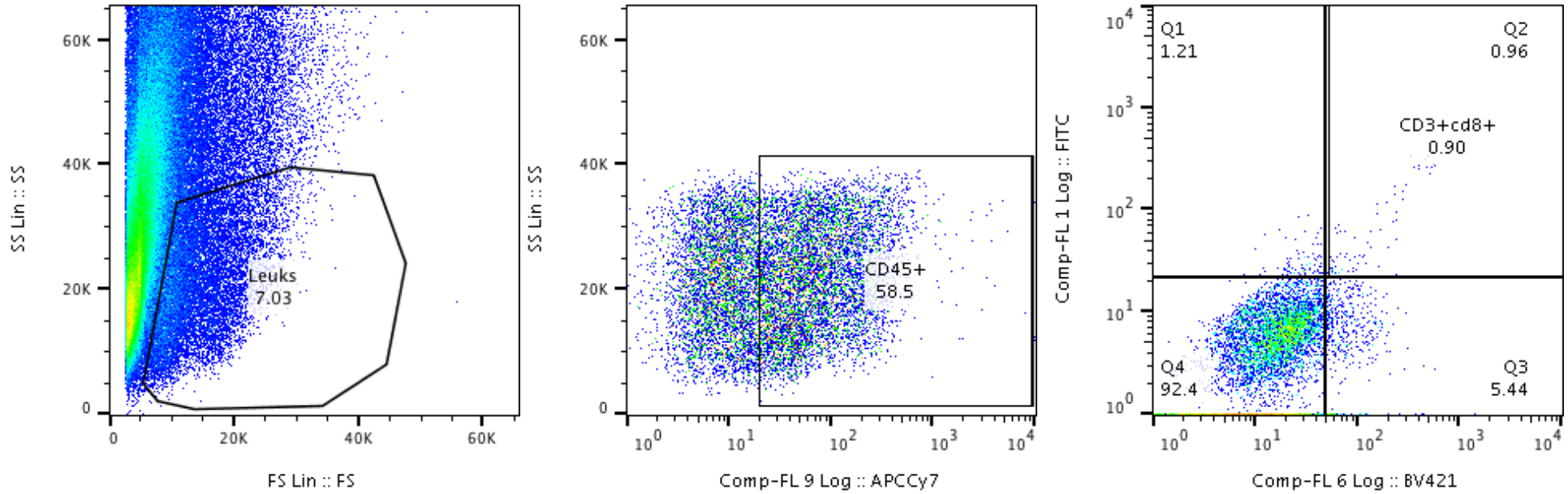

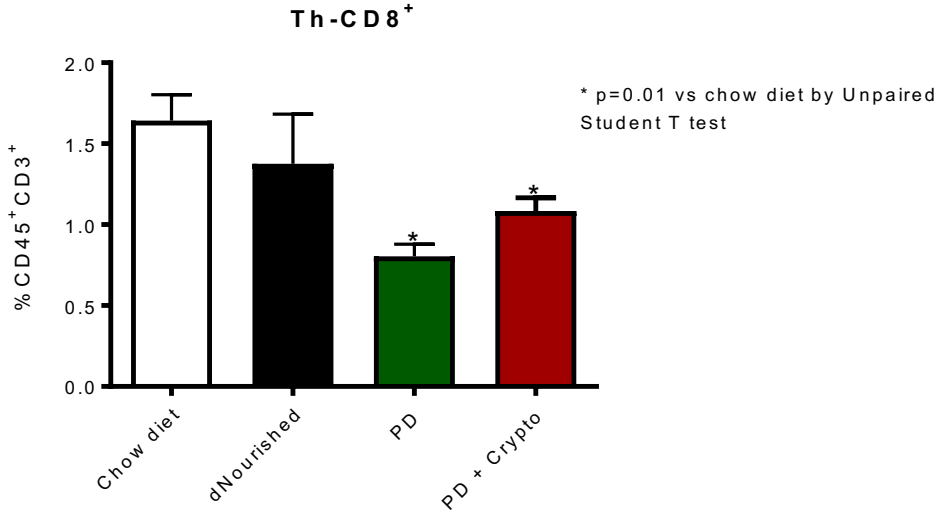

Undernutrition with or without *Crypto* infection reduces the NOS2 labeling in the meninges (need to be replicated)

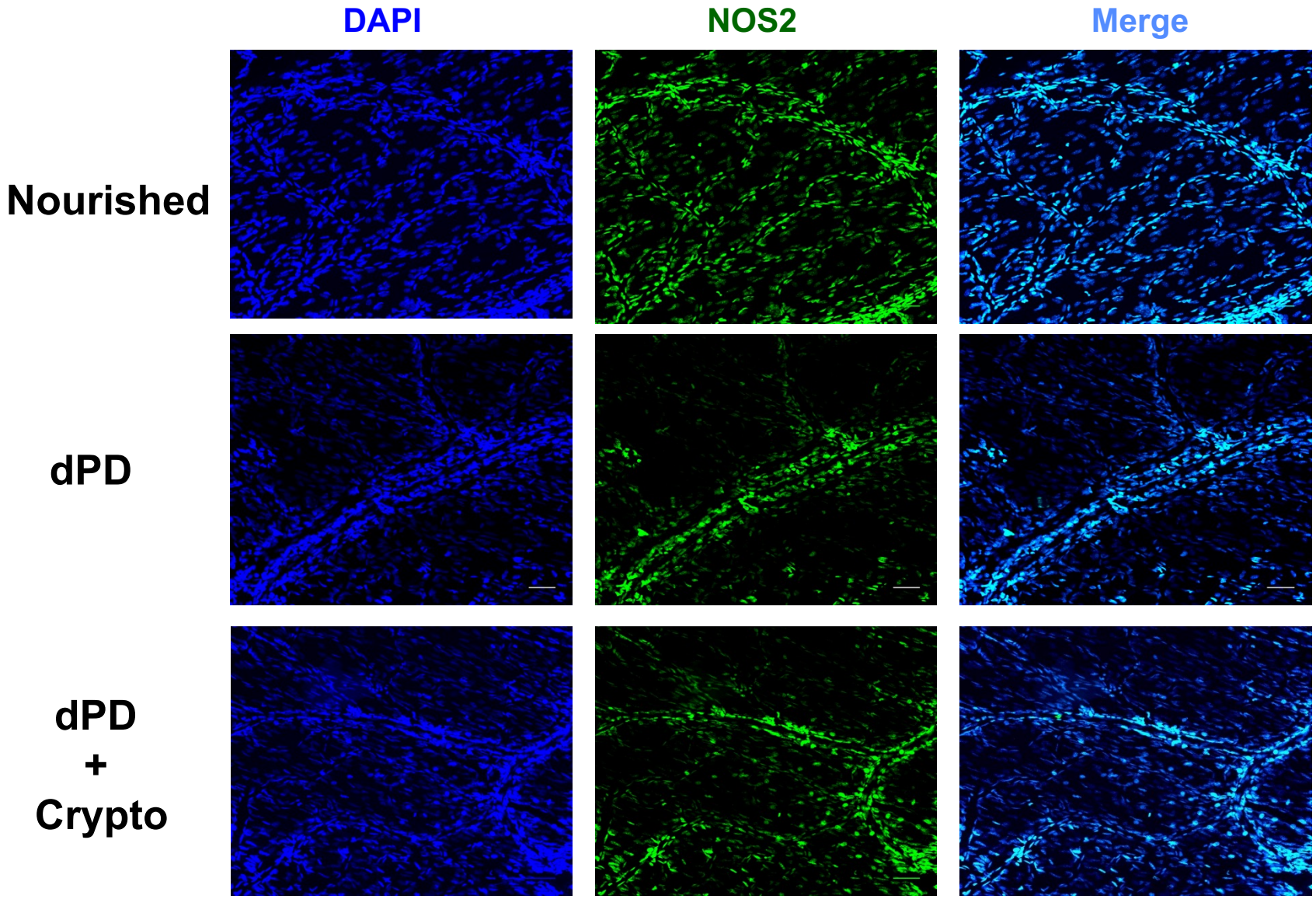

Scale bars: 50 μm

DAPI (4',6-diamidino-2-phenylindole) binds strongly to A-T rich regions in DNA.

Inflammatory biomarkers in the murine prefrontal cortex with representative immunostaining for IBA-1 and NF-Kb immunoblotting of the experimental mice after C. parvum infection and controls.

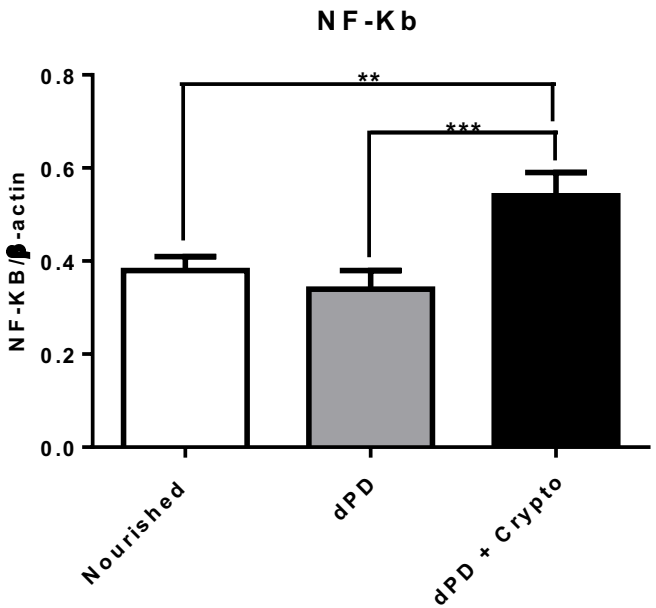

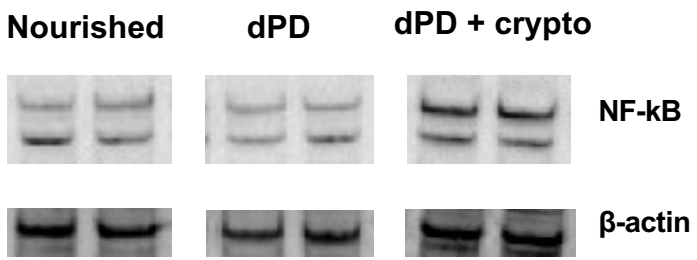

Oriá et al, Braz J Infec Dis, 2023

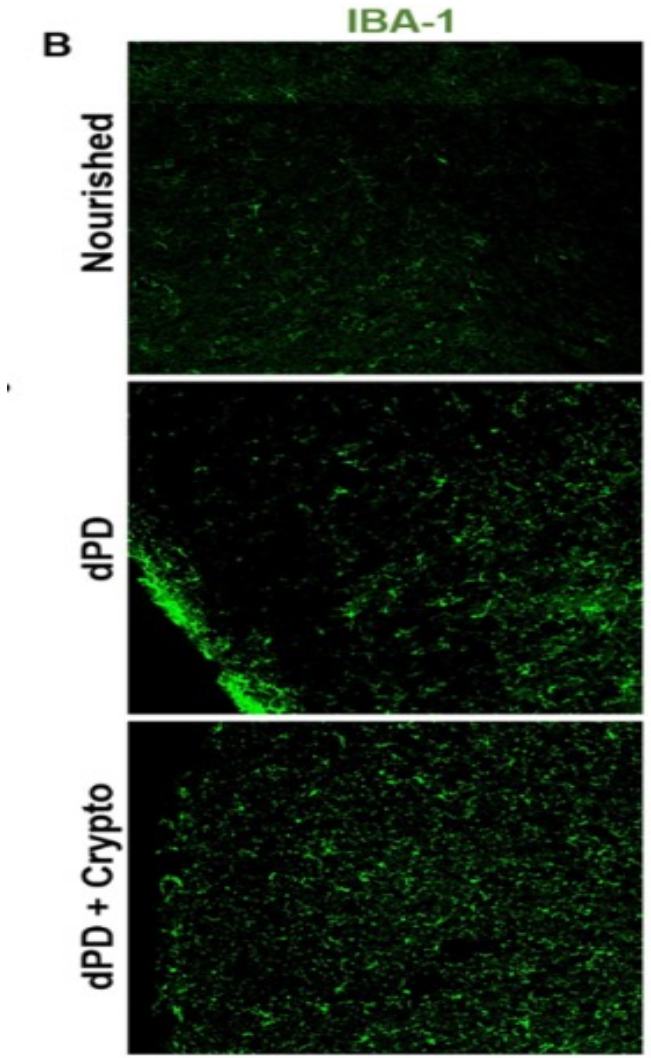

IBA-1=*ionized calcium-binding adaptor molecule 1*

Luminex assay of overall brain from C. parvum infected mice and controls (6 days post-infection)

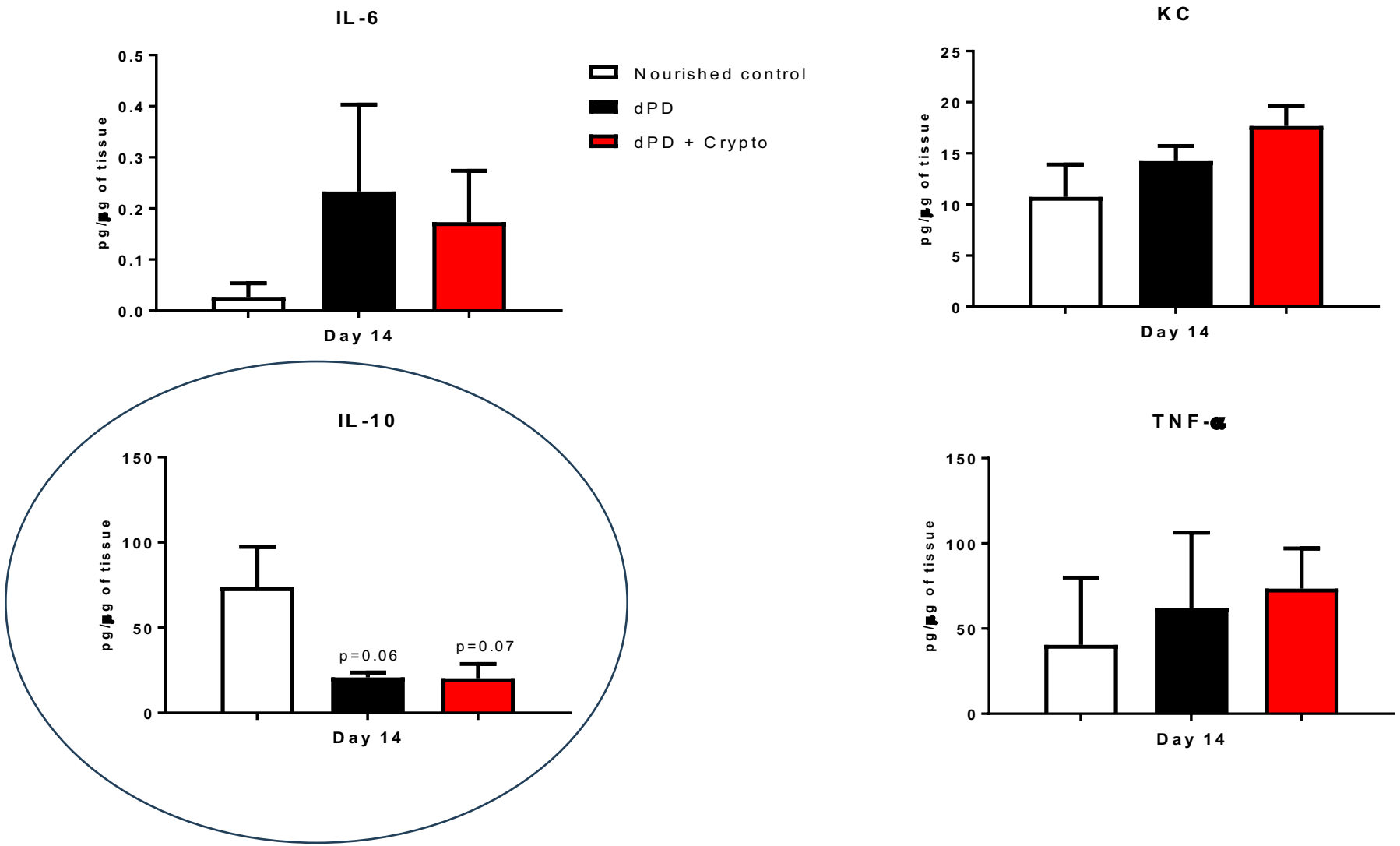

Enteric infection/malnutrition

- *C. parvum oocyst*

Gut-brain axis

↑ **Inflammatory cell activation**
Systemic inflammation

↑ **MPO and SAA**

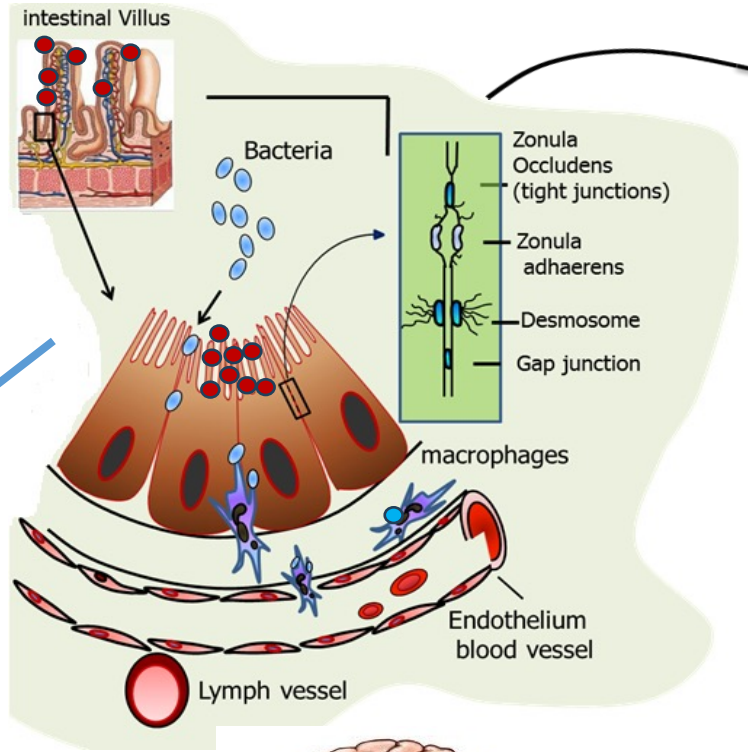

Epithelial junction permeability
Circulating bacterial products

BBB endothelial activation

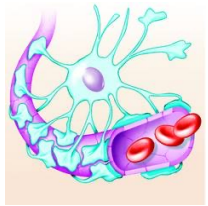

Neutrophil-released MPO?

Nutrient malabsorption
Cognitive decline (most semantic fluency)

MPO-related neuroinflammation

Increased MPO levels in the PFC

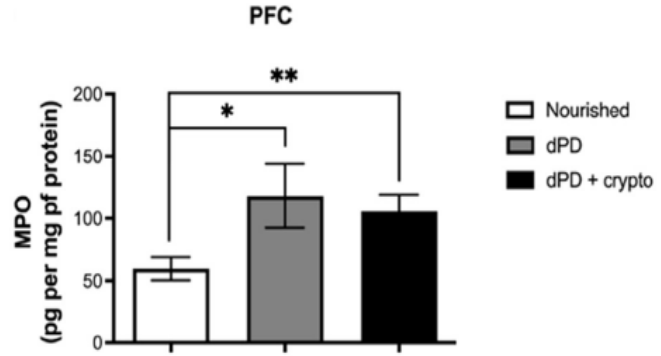

MPO positive cells were found in the hippocampus from a *C. parvum* infected mouse (need to be replicated)

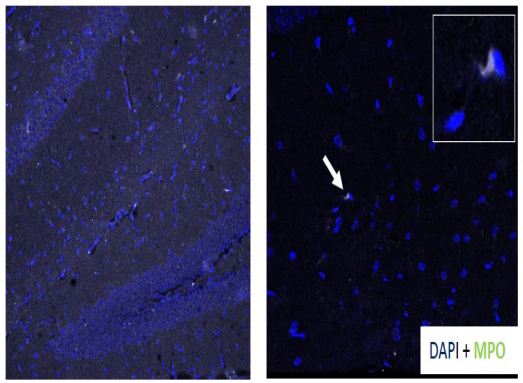

Adapted from Oriá et al, 2016, Nutrition Reviews.

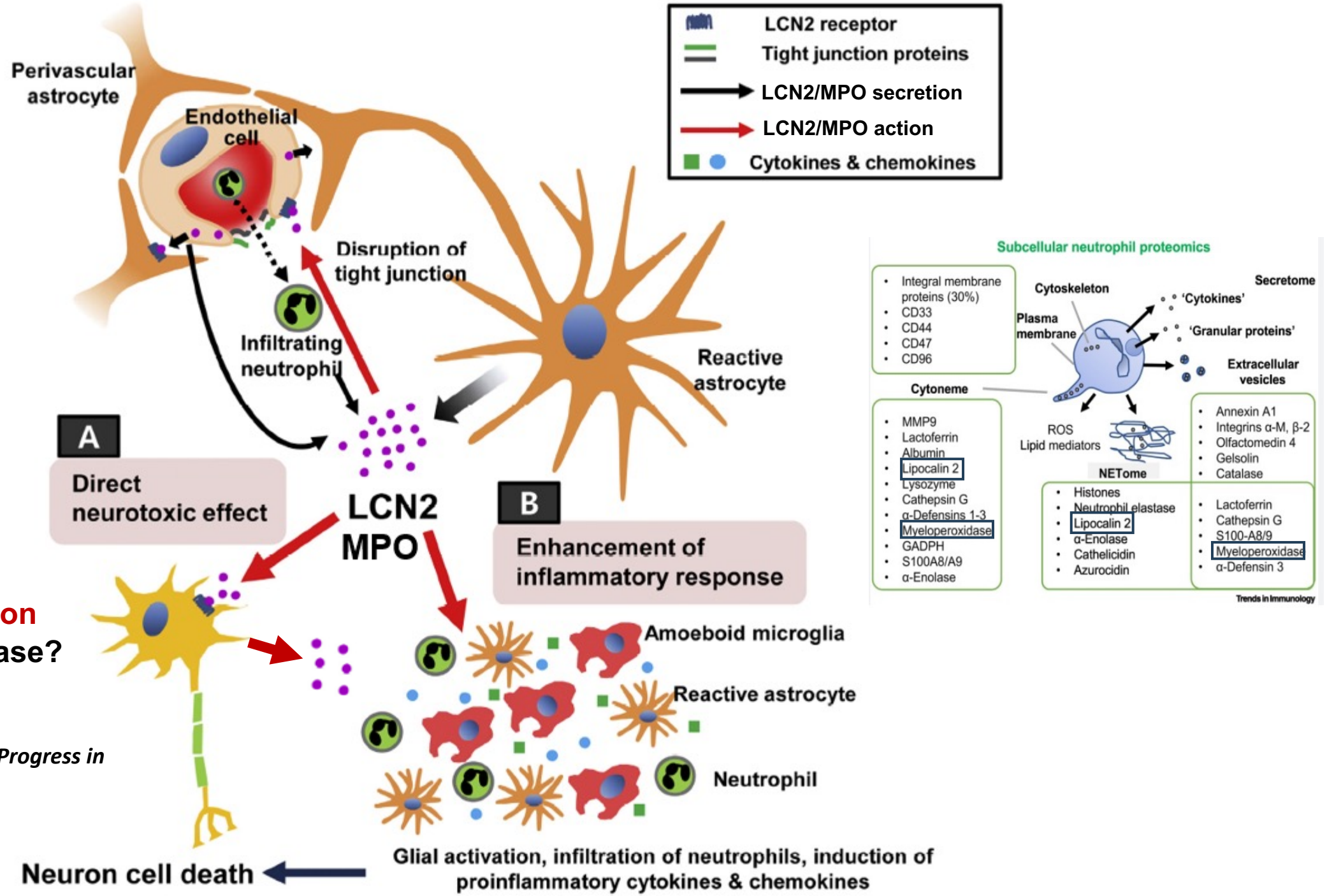

Adapted from Suk, K. Progress in Neurobiology, 2016

Conclusions 1

1. Undernourished mice showed profound impaired weight gain followed 8 days of dPD

2. Undernourished mice showed increase stool LPC-2 levels than nourished counterparts.

3. Crypto infection caused robust oocyst shedding at least up to 6 days post-infection.

4. Crypto-infected mice showed a significant weight loss 3 days post-infection compared with uninfected nourished and undernourished controls

5. Crypto-infected mice showed impaired tail and body length, markers of skeletal growth.

6. Crypto-infected mice showed reduced the frequency of CD8-T cells ($p<0.05$) compared with the nourished counterparts and showed IL-10 reduction in the overall brain.

7. Undernutrition with or without infection reduces NOS2 labeling in the brain meninges and increased labeling of IBA-1 cells in the PFC.

8. Undernourished *C. parvum* infected mice showed increased in NF-KB expression and MPO activity in the PFC compared to uninfected controls.

DIARRHEA
ENTERIC
INFECTION

Malnutrition
Growth and
Cognitive deficits

>Doubles the DALY

Guerrant et al Tr Paras 18: 191, 2002

Aim:
Break the cycle of diarrhea/malnutrition

Causal ?

1. **Genetic**
   (APOE alleles)
2. **Intervention**

   (ApoE mimetic peptides?)

APOE4 associates with lower diarrhea burdens (n=123 children; 246 alleles)

	Genotypes						Alleles		
APOE	**2/2**	**2/3**	**3/3**	**2/4**	**3/4**	**4/4**	**2**	**3**	**4**
Heavy Diarrhea % (n=64)	1.56 (1)	12.5 (8)	64.0 (41)	3.13 (2)	17.19 (11)	1.56 (1)	9.38* (12)	78.9 (101)	11.7 (15)
Low Diarrhea % (n=59)	0 (0)	X2↓ 5.09 (3)	62.71 (37)	0 (0)	X2↑ 32.2 (19)	0 (0)	2.54 (3)	82.2 (95)	15.2 (18)

*3x2 chi-square *p*=.033

Table 2. *ApoE genotype and allele frequencies (f) of cohort children (6–12 y) with different burdens of diarrhea in Gonçalves Dias (GD) shantytown, Fortaleza, northeast of Brazil (n = 72)*

	Genotypes						Alleles		
APOE	2/2	2/3	3/3	2/4	3/4	4/4	2	3	4
Group 1, *n* (*f*%)	01 (3.12)	03 (9.37)	21 (65.63)	02 (6.25)	05 (15.63)	00 (00)	07 (10.9)	50 (78.2)	07 (10.9)
Group 2, *n* (*f*%)	00 (00)	05 (12.5)	21 (52.5)	00 (00)	14 (35)	00 (00)	05 (6.2)	61 (76.3)	14 (17.5)
Total, *n* (*f*%)	01 (1.4)	08 (11.1)	42 (58.3)	02 (2.8)	19 (26.4)	00 (00)	12 (8.3)	111 (77.1)	21 (14.6)

Group 1, cohort children with ≥ the mean episodes of diarrhea (n = 32); group 2, cohort children with < the mean episodes of diarrhea (n = 40). Mean episodes of diarrhea in the first 2 y of life = 9.28.

Introduction

Apolipoprotein E

(ApoE), a 35 KDa plasma protein synthesized mainly in the liver and in the brain, is critically involved in cholesterol transport and metabolism.

(Mahley & Rall, 2000; Yamouch et al, 1999, Liberman, et al, 2002).

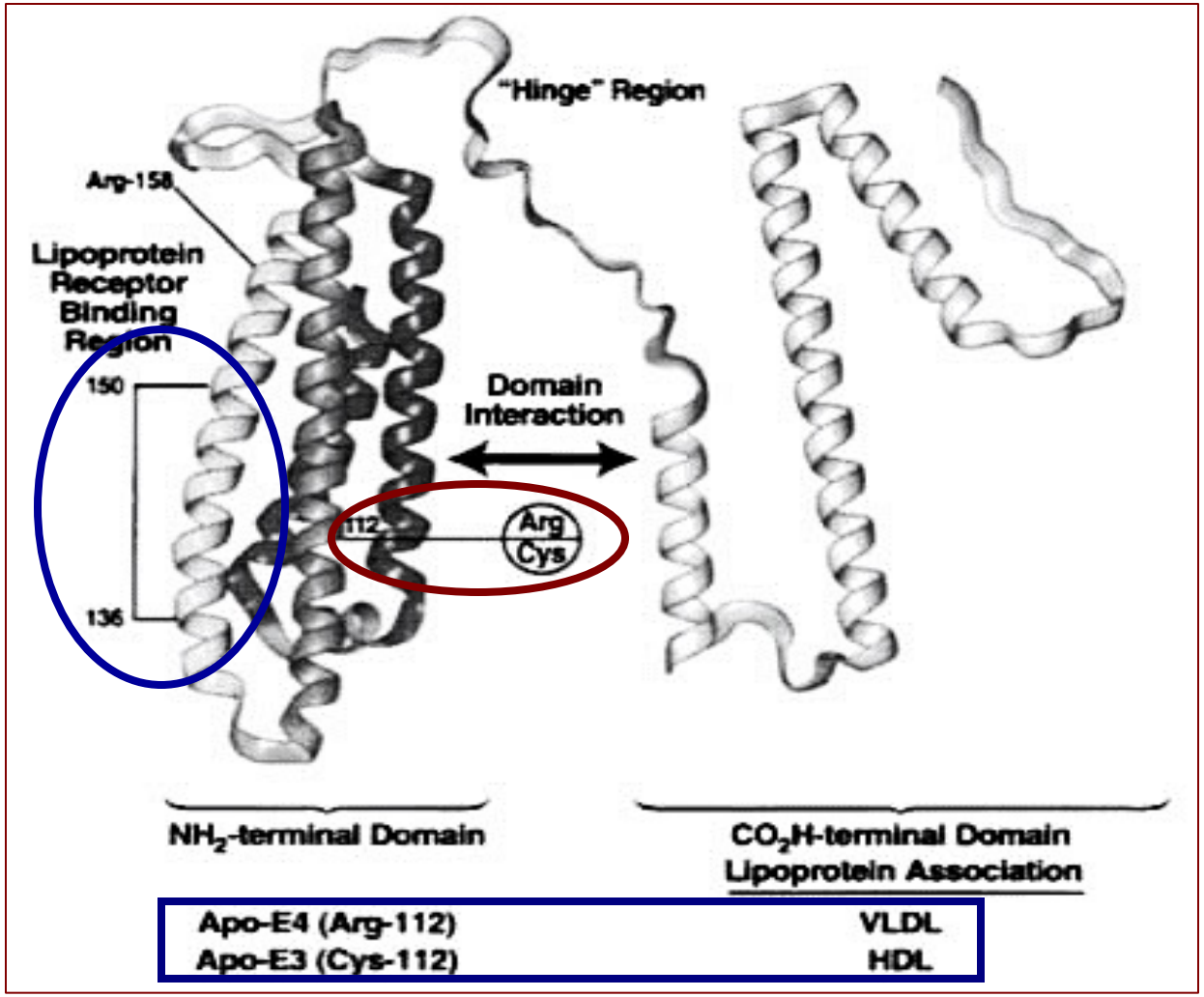

Isoelectric separation of Apolipoprotein E

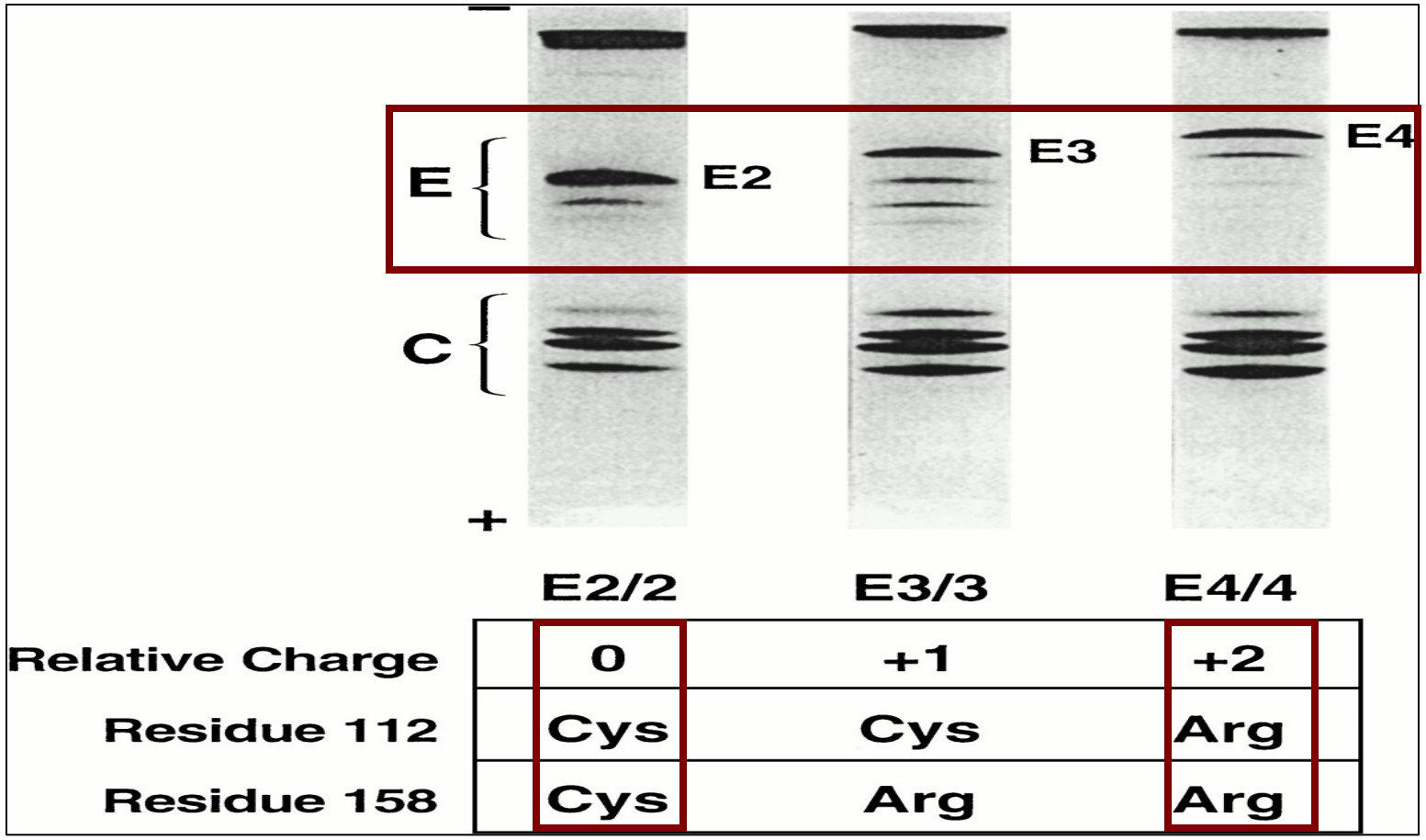

Isoelectric separation of the VLDL, after lipid extraction, showing 3 apoE homozygous patterns, E2/2, E3/3 & E4/4.

Mahley & Rall, 2000

Three-dimensional structure of ApoE

Affinity to the LDL receptor

APOE2 is the only isoform which contains Cys-158

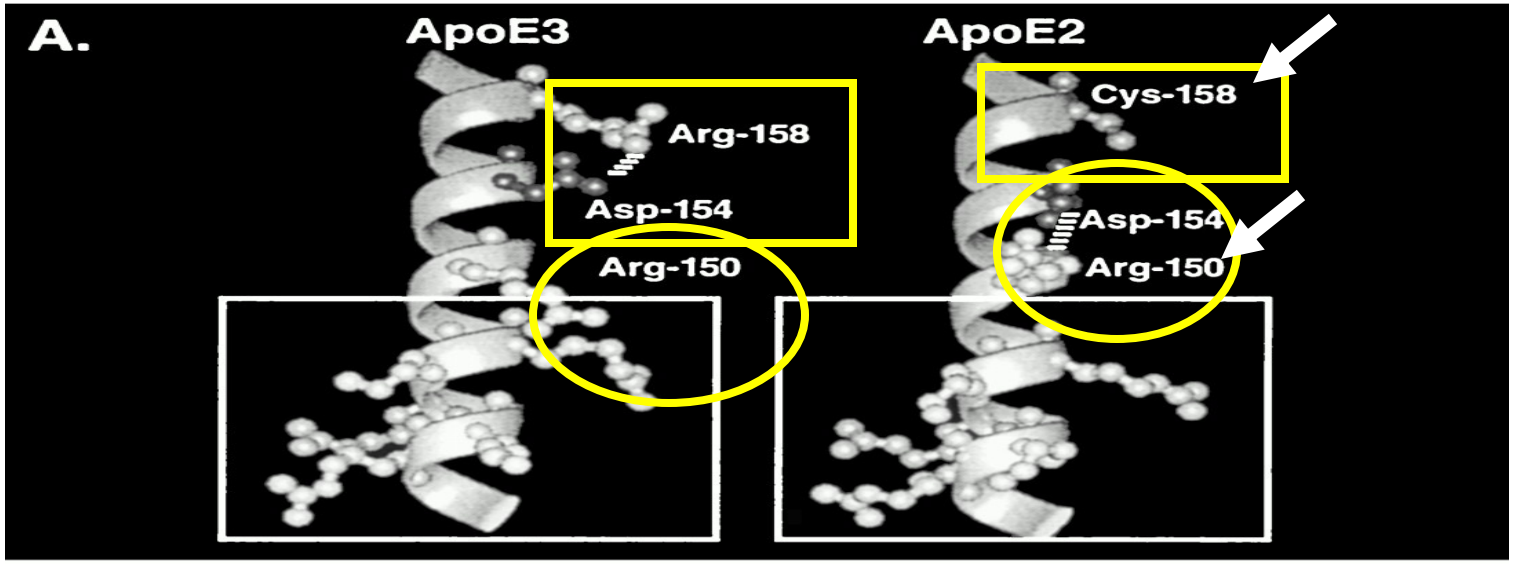

Affinity to the lipoprotein

APOE4 is the only isoform which contains Arg-112

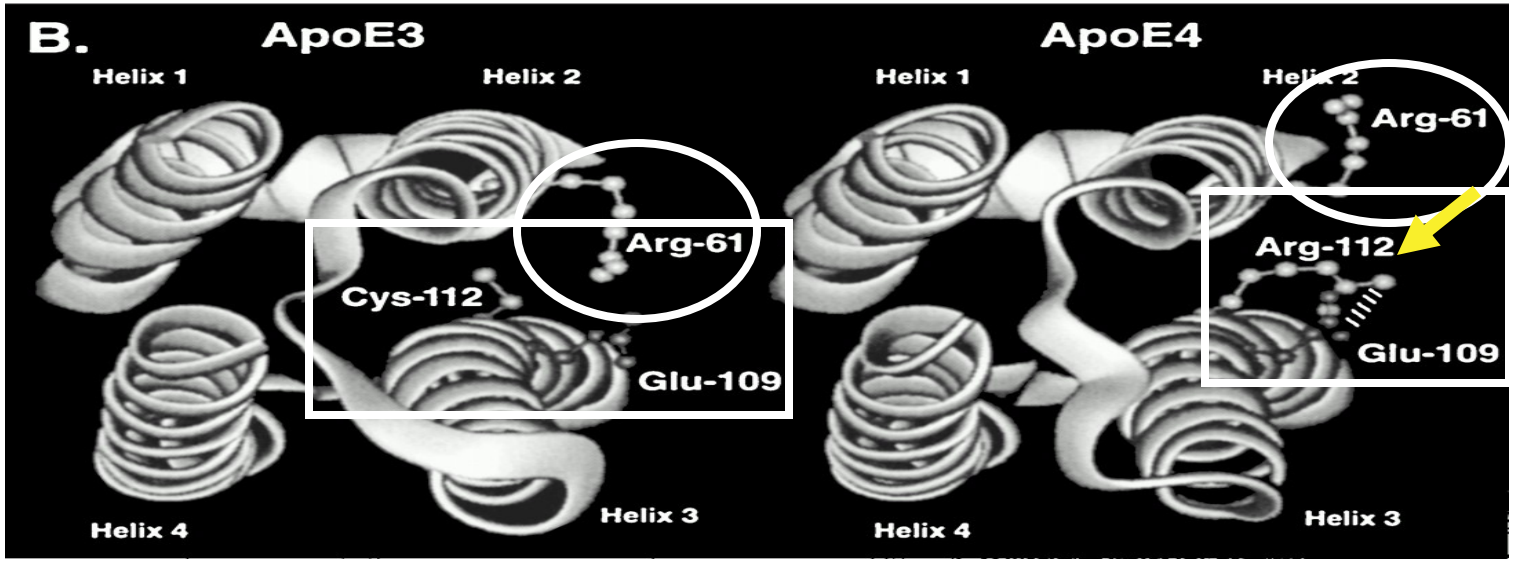

Mahley et al, Journal of Lipid Research, 2009

Effect of APOE alleles on lipid parameters

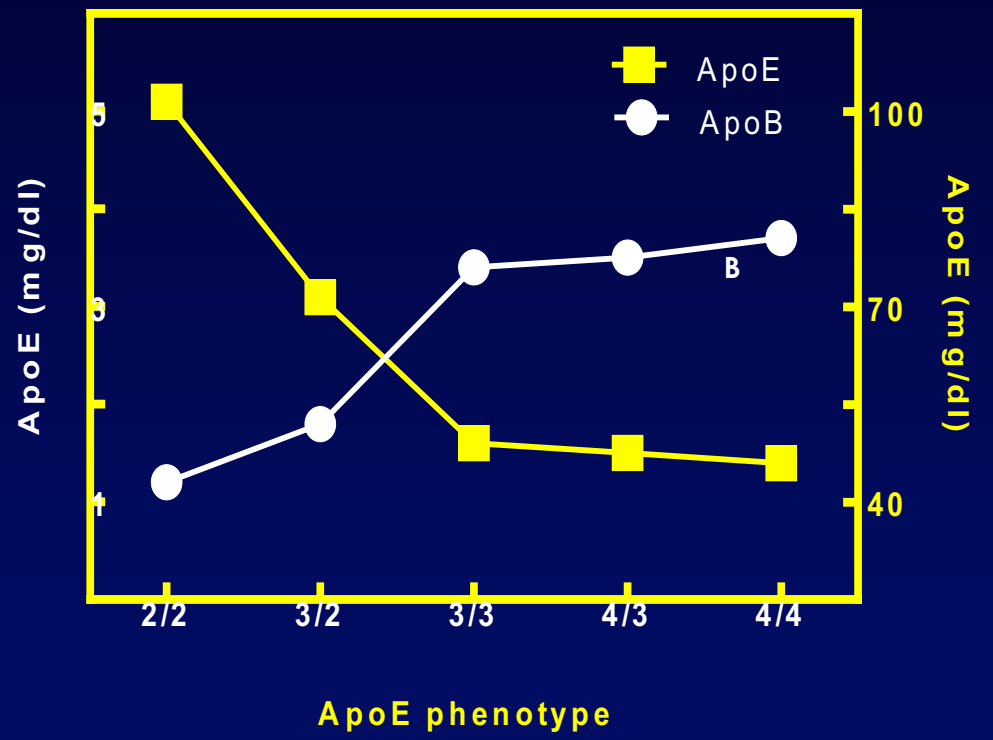

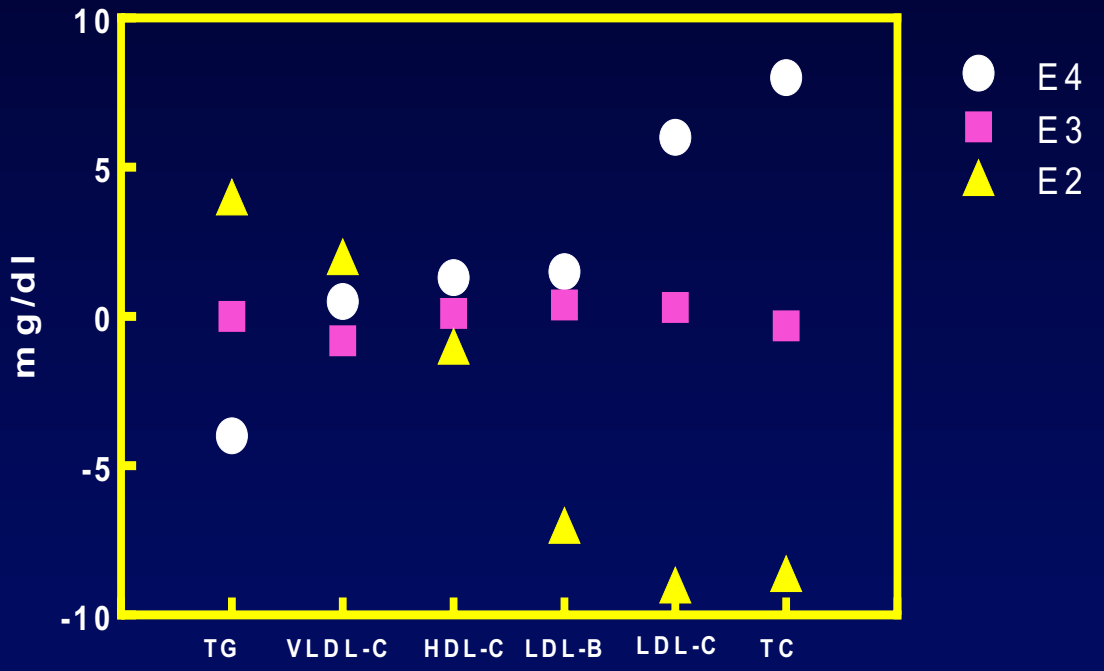

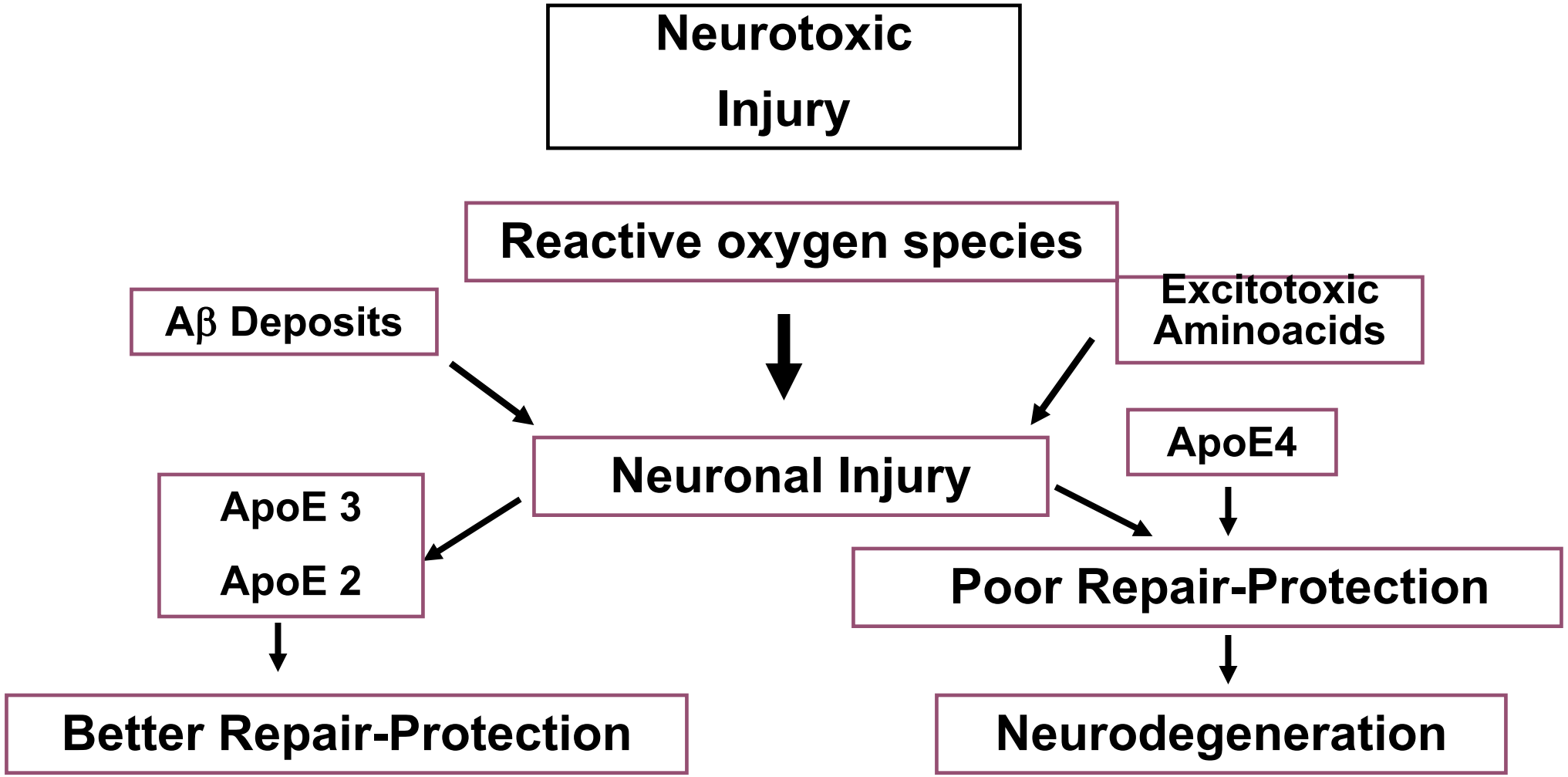

Mahley et al, 2000

Methodology/design

- 3 week-old C57BL/6 (wild-type, APOE ko, APOE3 TR, APOE4 TR) mice

- Diets for 2 weeks:
  - Nourished mice (20% of protein diet)
  - Malnourished mice (2% of protein diet)

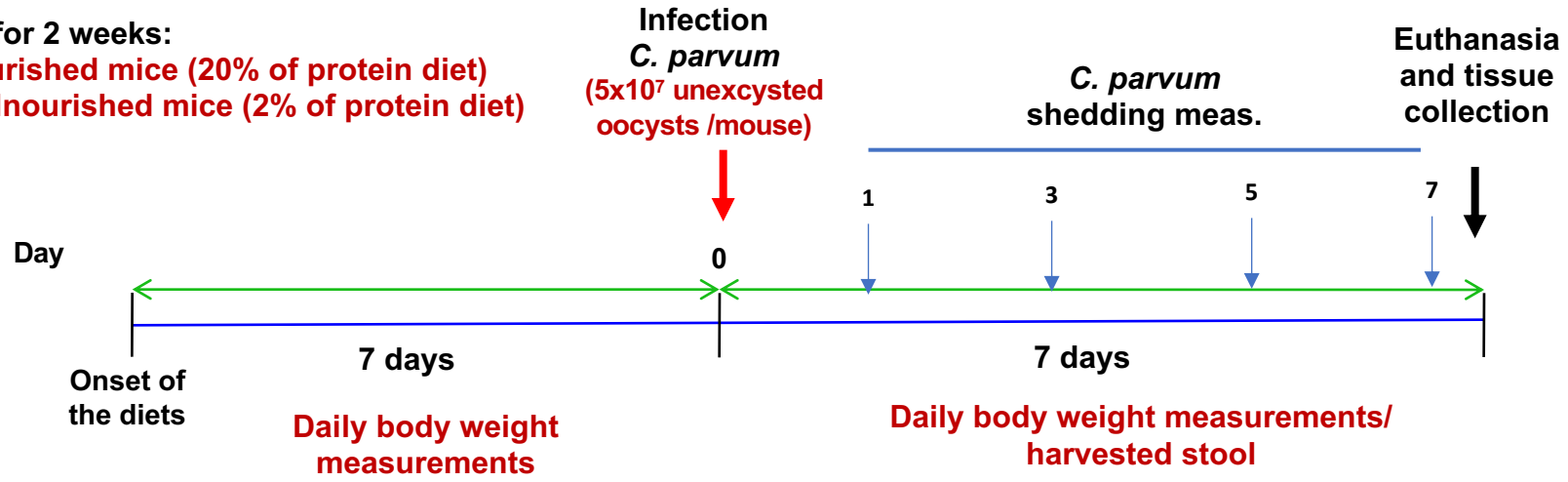

After infection, stools were assessed for *C. parvum* oocyst shedding and ileal inflammatory biomarkers (IL-1β, IFN-γ, Il-17, and TNF-α by Luminex), CAT-1, arginase-1, TLR-9, and iNOS (qRT-PCR) transcriptional levels. Mouse body and tail length were measured at the endpoint.

APOE target replacement (TR) mice

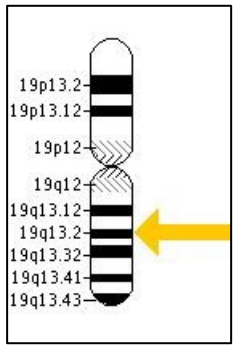

blastocyst

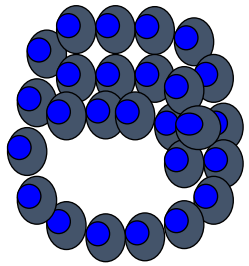

embryonic stem cells
E14TG2a

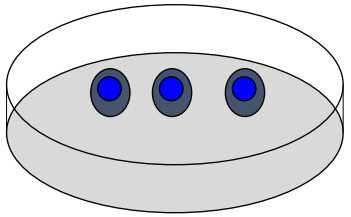

genetic plasmid
pHEG-1

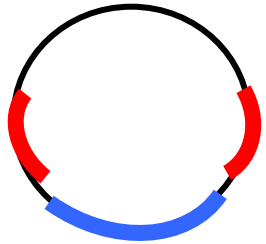

Target gene
insertion

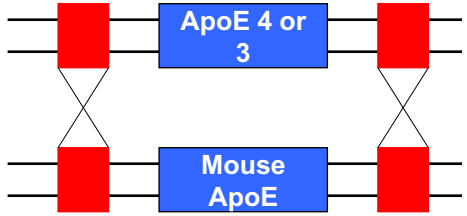

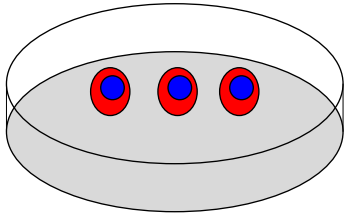

Transfected cells
selection by Southern
Blotting

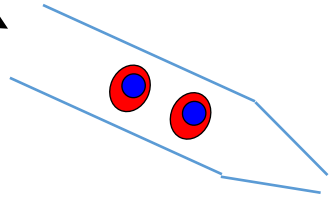

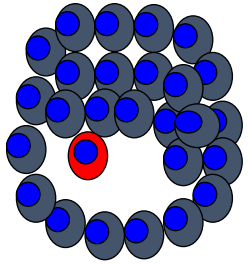

Blastocyst implantantion

F2 generation

List of study primers para qRT-PCR

Primers	Sequence (5’-3’)
β-actin	AATTTCTGAATGGCCCAGGT TTTGTGTAAGGTAAGGTGTGC
Arginase-1	TCTGCCAAAGACATCGTGTA GGTAGCTGAAGGTCTCTTCC
CAT-1	CACTGCTGATCTGTGTACCT GTGGGGACATAAGATGCTCA
RNA 18s from *C. parvum*	CTGCGAATGGCTCATTATAACA AGGCCAATACCCTACCGTCT
iNOS	TCCTGGACATTACGACCCCT AGGCCTCCAATCTCTGCCTA
TLR9	TGGTGTTGAAGGACAGTTCTCTC CACTCGGAGGTTTCCCAGC

ApoE deficiency leads to impaired growth. APOE4 TR mice recover the catch-up growth faster following *C. parvum* infection.

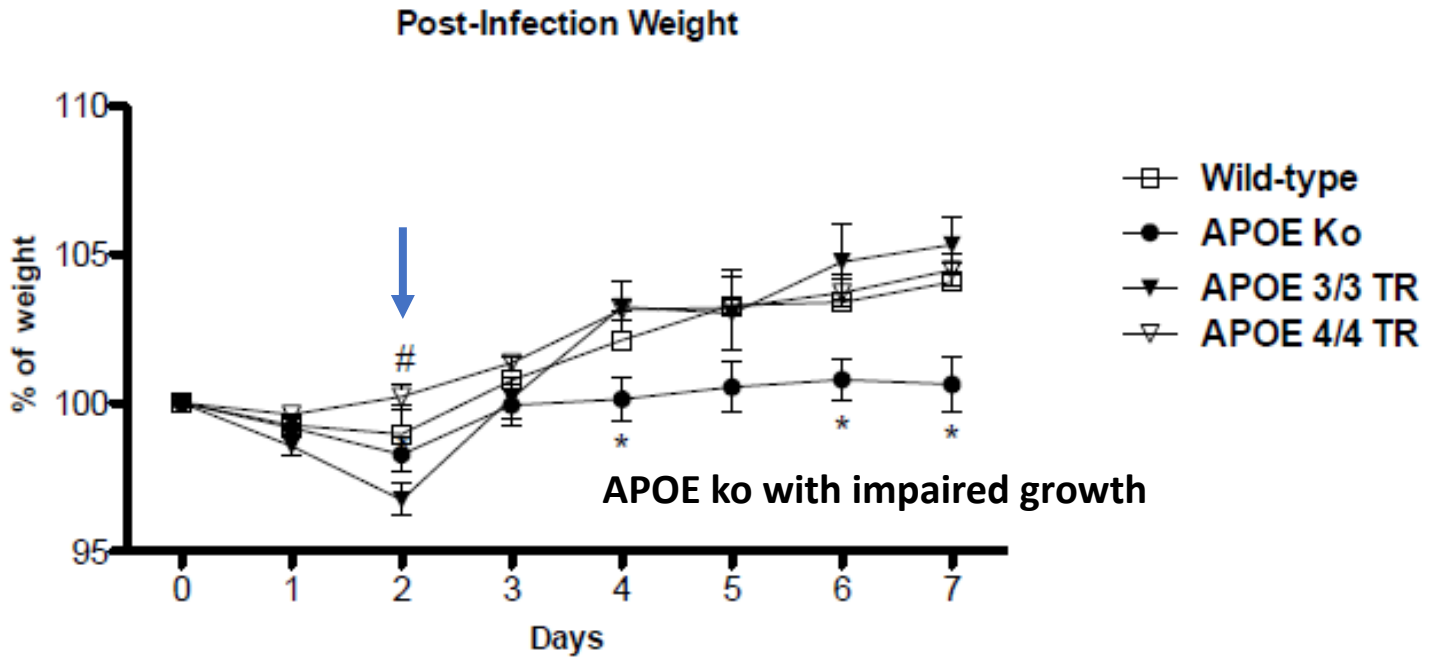

* p<0.05 vs all

# p<0.05 APOE 4/4 TR vs APOE 3/3 TR and APOE Ko

Representative histology of ileal samples from *C. parvum*-infected undernourished mice and controls according to APOE genotype

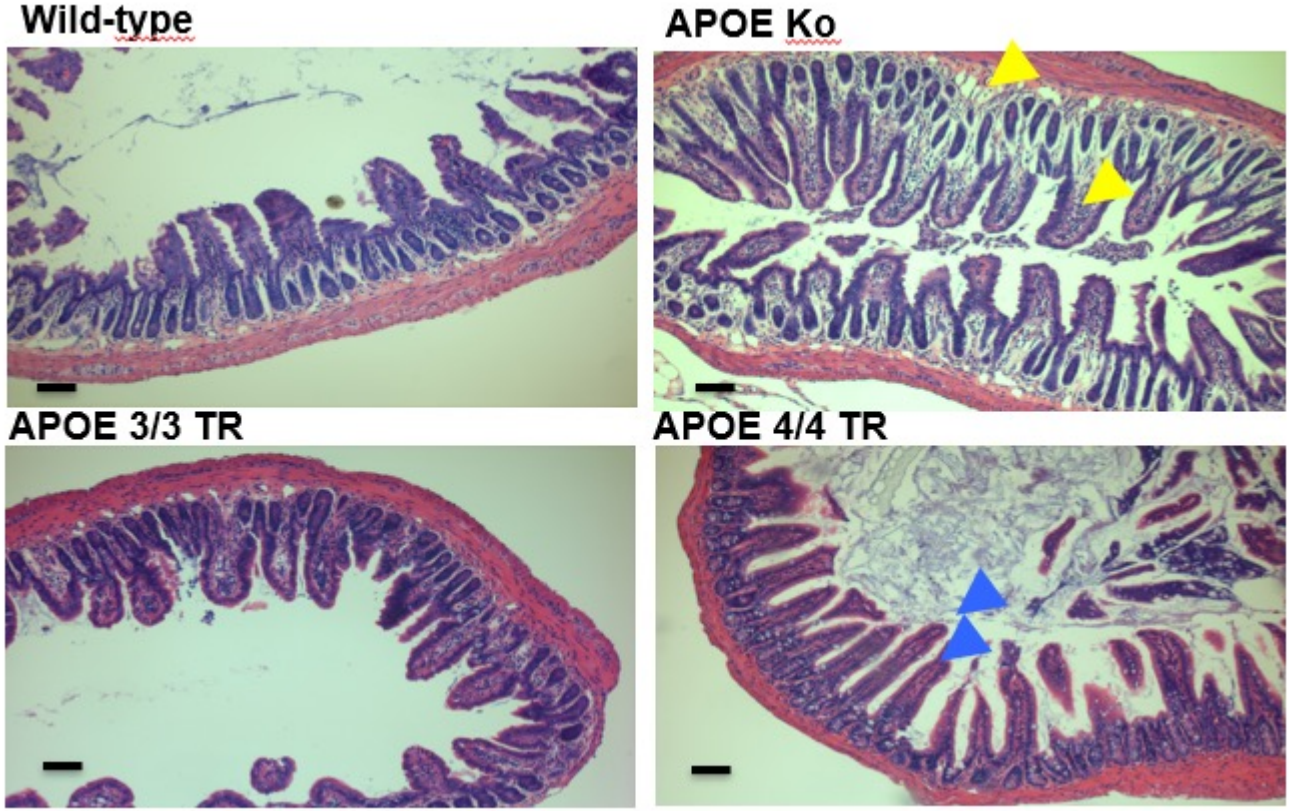

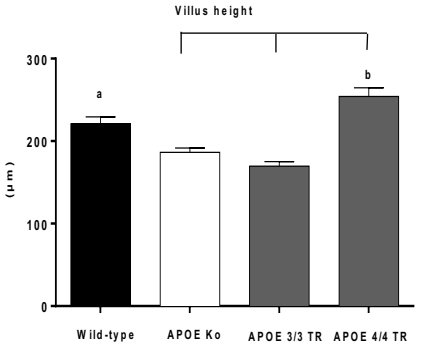

a: p<0.05 Wild-type vs APOE Ko and APOE 3/3 TR by ANOVA and Bonferroni
b: p<0.0001 APOE 4/4 TR vs APOE Ko and APOE 3/3 TR by ANOVA and Bonferroni

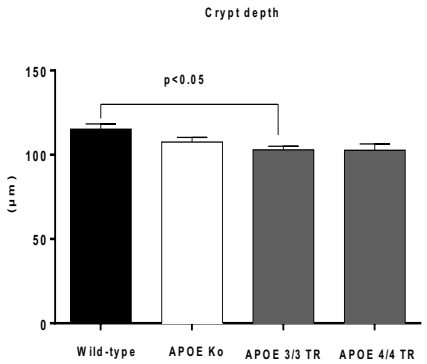

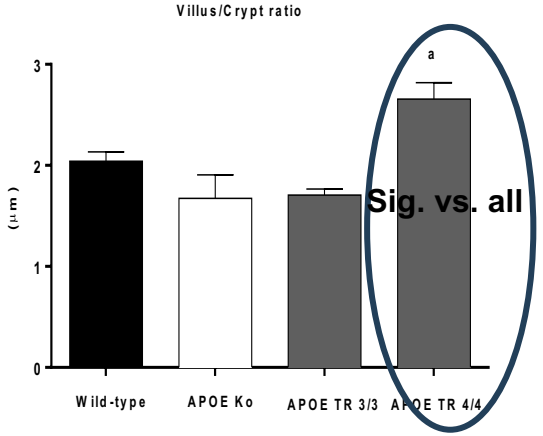

a: p<0.05 APOE TR 4/4 vs all by ANOVA e Bonferroni

Scale bar: 10 µm.

Yellow arrow heads point to increased inflammation and blood vessel congestion in the ileum from APOE ko mice. Blue arrow heads indicate improved villus architecture in the ileum from APOE 4/4 TR mice

Fecal shedding of parasites in weaned undernourished C57BL/6 mice orally inoculated with 10^7 -unexcysted *C. parvum* oocysts per mouse on day 7 after the onset of the low protein diet.

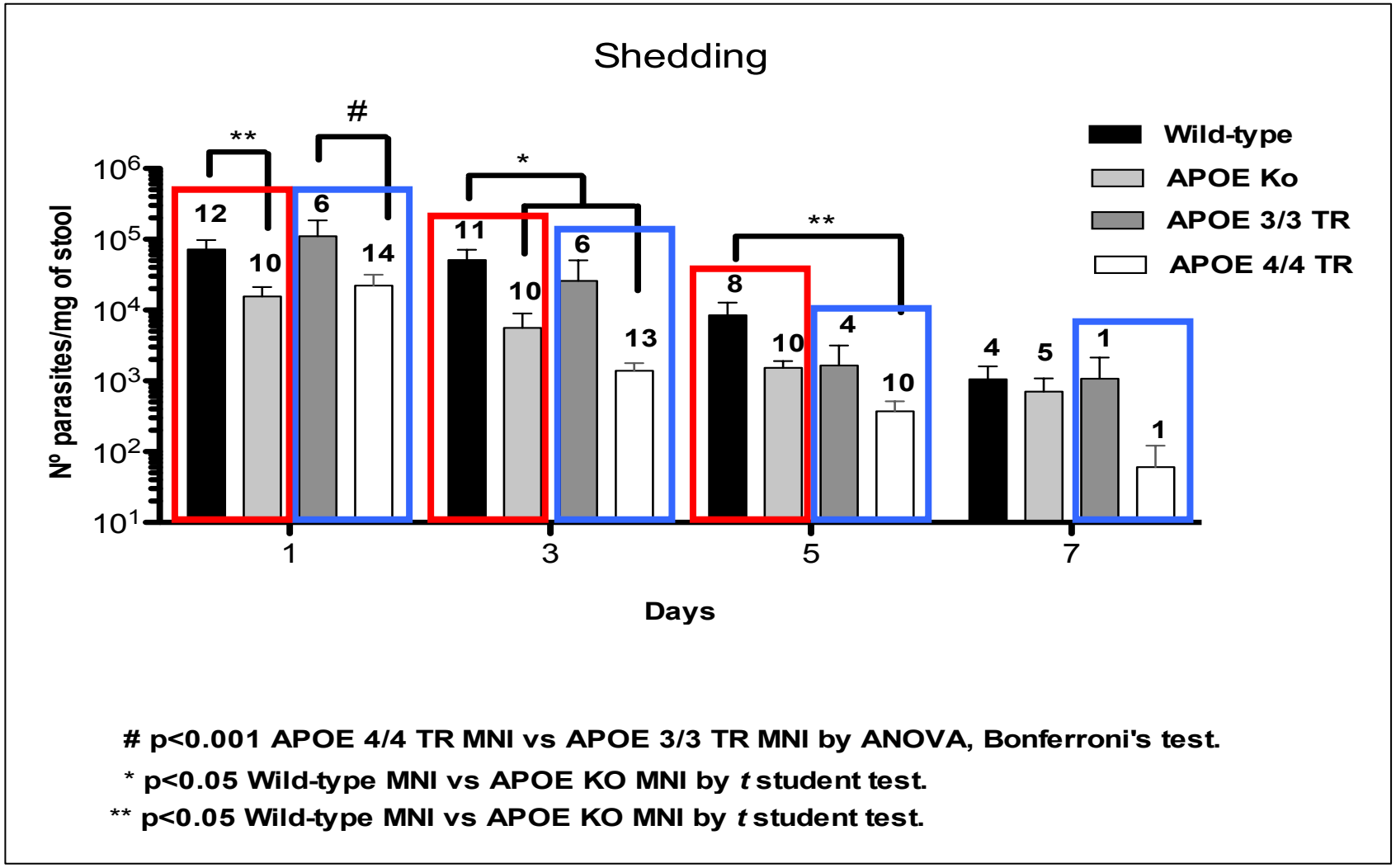

Results are shown in a log scale a mean±SEM.
Data were expressed as number of parasites per mg of stool. N above the bars means the number of mice still showing oocyst shedding

Significant reduction of *C. parvum* stool shedding in APOE4 TR mice following infection

Days	Wild-type	APOE Ko	APOE TR 3/3	APOE TR 4/4
Day 1	12 (100%)	10 (100%)	6 (100%)	14 (100%)
Day 3	11 (91.67%)	10 (100%)	6 (100%)	13 (92.85%)
Day 5	8 (66.67%)	10 (100%)	4 (66.67%)	10 (71.42%)
Day 7	4 (33.33%)	5 (50%)	1 (16.67%)	1 (7.14%)

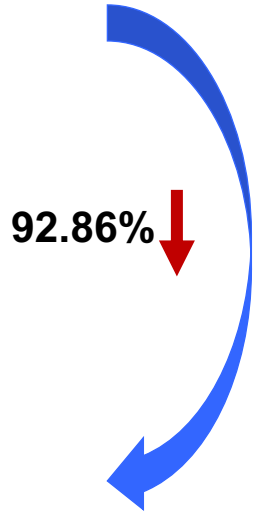

Luminex assay of ileal inflammatory markers from C57BL6J wild-type, APOE ko, APOE3 and APOE4 TR mice

IL-1β

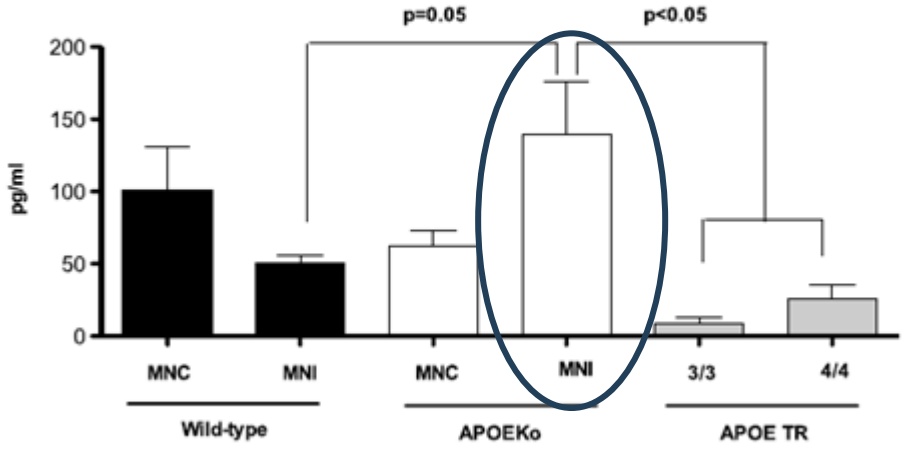

IL-17

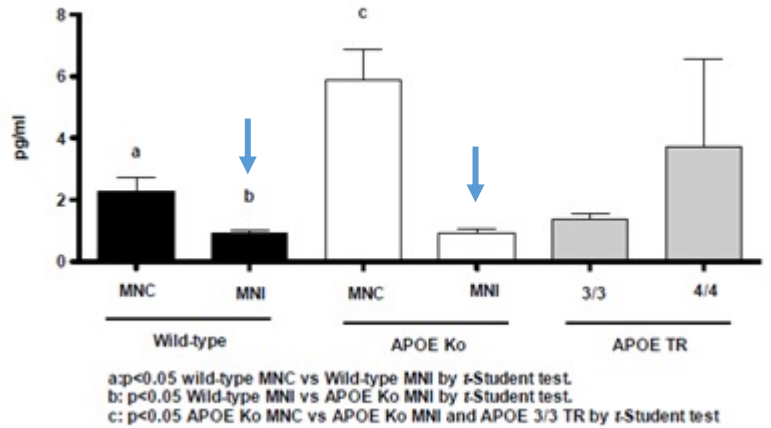

a:p<0.05 wild-type MNC vs Wild-type MNI by t-Student test.
b: p<0.05 Wild-type MNI vs APOE Ko MNI by t-Student test.
c: p<0.05 APOE Ko MNC vs APOE Ko MNI and APOE 3/3 TR by t-Student test

IFN-γ

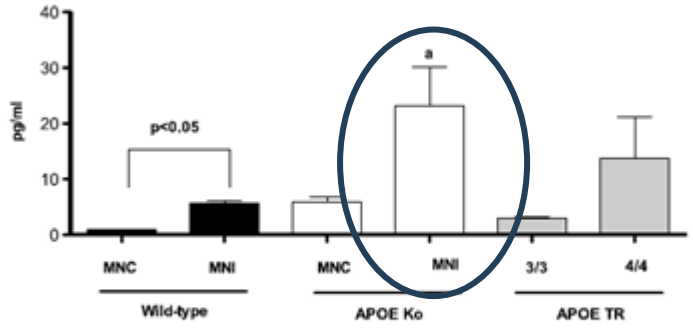

a:p<0.05 APOE KO MNI vs APOE KO MNC, wild type MNI and APOE TR 3/3 MNI by ANOVA and Bonferroni

TNF-α

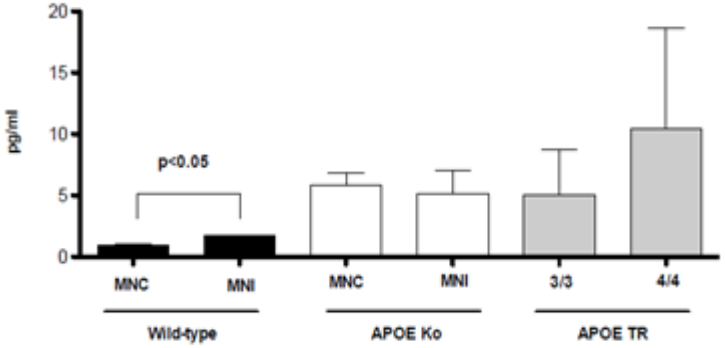

Lipid profile of experimental undernourished mice following *C. parvum* infection (orally infected with 10^7 unexcysted oocysts).

Analytes (mg/dL)	Wild-type (n=5)	ApoE Ko (n=5)	ApoE TR 4/4 (n=5)	ApoE TR 3/3 (n=4)
Total Cholesterol	60.8 ± 18.5	615.8 ± 69.6*	112 ± 16.9†	96.75 ± 14.0
HDL	52 ± 9.3	50 ± 5.7	58 ± 6.2**	47 ± 7.8
LDL	29.80 ± 6.5	576 ± 65.8***	45.8 ± 10.4	38.50 ± 7.0
Triglycerides	53.20 ± 17	59 ± 4.0#	48.6 ± 8.0	68.5 ± 24.0

* *p<0.001 ApoE Ko vs all*
** *p=0.05 ApoE TR 4/4 vs ApoE TR 3/3*
*** *p<0.001 ApoE Ko vs all*
\# *p<0.05 ApoE Ko vs ApoE TR 4/4*
† *P<0.05 vs wild-type mice*

APOE4 TR mice showed increased ileal Arg1, TLR9, and CAT-1 transcriptional levels. Arg1 is key for mucosal recovery after following *C. parvum* infection

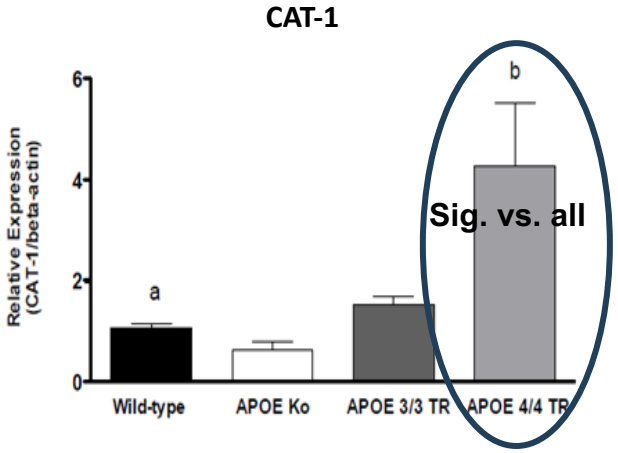

a: p<0.05 Wild-type vs APOE Ko by ANOVA and Bonferroni
b:p<0.05 APOE 4/4 TR vs all by ANOVA and Bonferroni

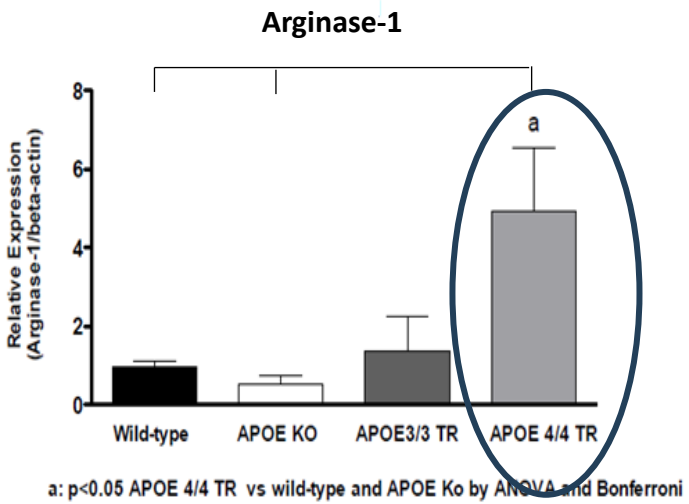

a: p<0.05 APOE 4/4 TR vs wild-type and APOE Ko by ANOVA and Bonferroni

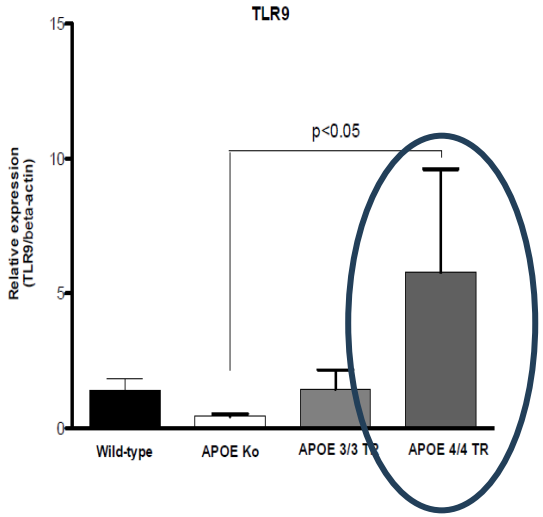

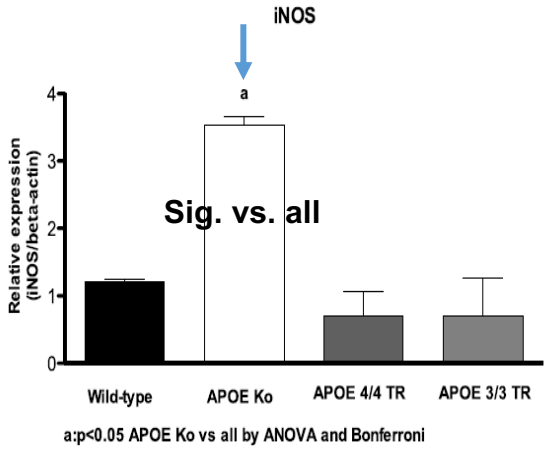

a:p<0.05 APOE Ko vs all by ANOVA and Bonferroni

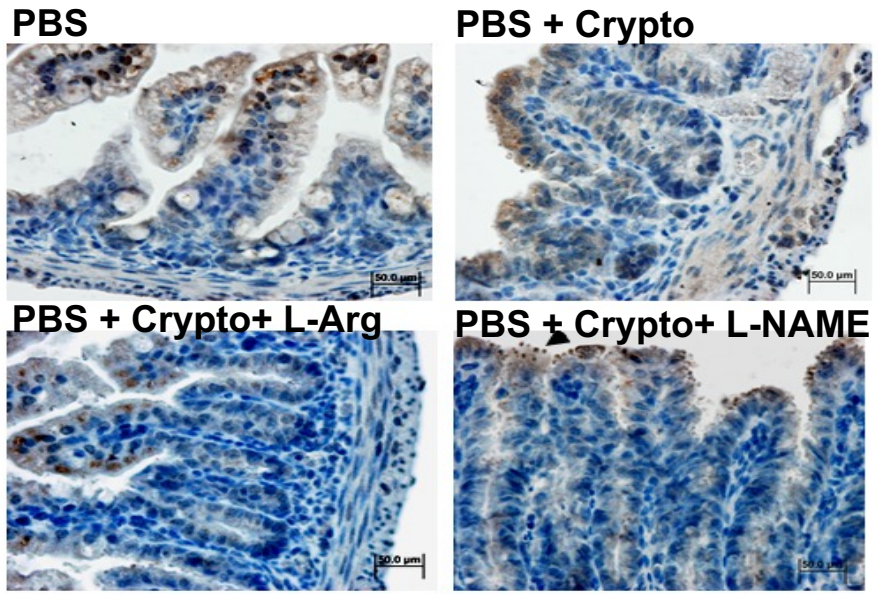

Castro et al, Nutrition, 2012

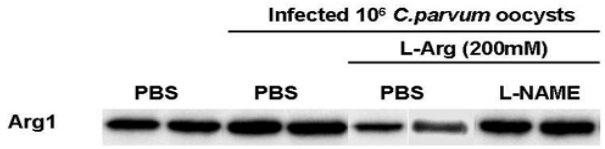

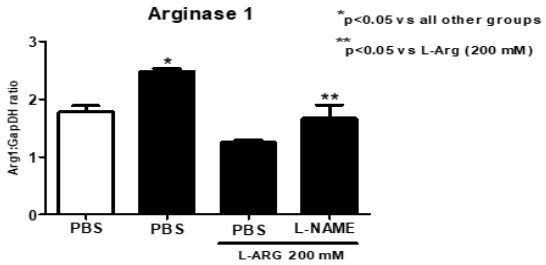

Conclusions 2

1. APOE-deficient mice had significantly less *C. parvum* oocyst shedding measured by quantitative PCR in stools on the 1st and 3rd days post-infection, when the infection peaks.

2. APOE-deficient mice had greater inflammatory cytokine responses and mucosal atrophy in the ileal tissue one week-post inoculum, accompanied by greater weight deficits following 7 days of infection.

3. APOE4 mice had increased ileal TLR9 transcripts compared with APOE knockout mice. TLR9-immune mediated responses have been found important to control C. parvum infection in a neonatal mouse model.

4. APOE4 contributes to elimination of *C. parvum* infection with a more regulated inflammatory response compared to the uncontrolled cytokine production noted in ApoE deficient mice.

5. APOE4 has been shown to up-regulate ileal L-arginine cationic protein transporter (CAT-1) and arginase 1 transcription levels.

mRNA Microarray of Gene Expression in undernourished non-infected vs infected mice

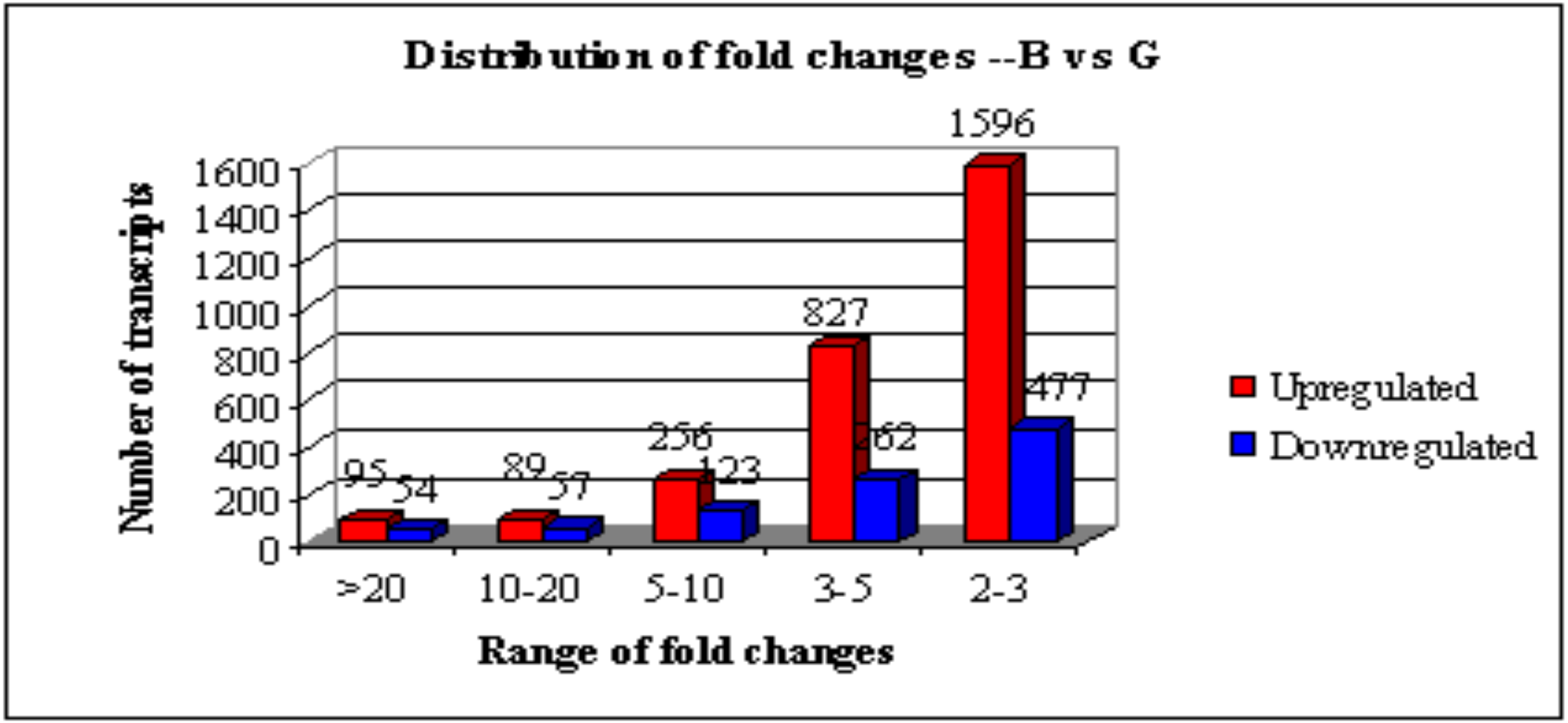

Upregulation	Gene list (MN vs MN 10e6 crypto infected)
>1000 fold	RIKEN cDNA 4933439A12 gene
>100 fold	serine (or cysteine) proteinase inhibitor, clade A, member 1a, inactive X specific transcripts, secreted phosphoprotein 2, inactive X specific transcripts, **bone morphogenetic protein 7**, ---, N-acetylneuraminate pyruvate lyase, inactive X specific transcripts, alpha fetoprotein, **glutathione S-transferase**, alpha 3
61-100 fold	---, coagulation factor X, NADPH oxidase 4, NADPH oxidase 4, RIKEN cDNA E130002L11 gene, eukaryotic translation initiation factor 2C, 3, **fibroblast growth factor receptor 4**, restin (Reed-Steinberg cell-expressed intermediate filament-associated protein), alpha fetoprotein, **transthyretin**, fibrinogen, B beta polypeptide
31-60 fold	afamin, solute carrier family 39 (metal ion transporter), member 8, **claudin 8**, chymotrypsinogen B1, phosphoglycerate mutase 2, mucolipin 3, Ros1 proto-oncogene, leucine rich repeat protein 1, neuronal, ---, arylacetamide deacetylase (esterase), transthyretin, fibrinogen, alpha polypeptide, alpha fetoprotein, opposite strand transcription unit to Stag3, **folate receptor 1 (adult)**, neuritin 1, antigen p97 (melanoma associated) identified by monoclonal antibodies 133.2 and 96.5, RIKEN cDNA 3110057O12 gene, Similar to Lactase-phlorizin hydrolase precursor (Lactase-glycosylceramidase) (LOC226413), mRNA, ATP-binding cassette, sub-family A (ABC1), member 13, AT rich interactive domain 4B (Rbp1 like), coagulation factor X, ectonucleotide pyrophosphatase/phosphodiesterase 3, ectonucleotide pyrophosphatase/phosphodiesterase 3, transthyretin, mucolipin 3, solute carrier family 19 (sodium/hydrogen exchanger), member 3, renin binding protein, **transthyretin**, afamin, RIKEN cDNA 2610019F03 gene, sema domain, immunoglobulin domain (Ig), and GPI membrane anchor, (semaphorin) 7A, galactosylceramidase, **lecithin-retinol acyltransferase (phosphatidylcholine-retinol-O-acyltransferase)**, dipeptidylpeptidase 7
20-30 fold	DNA-damage inducible transcript 3, alpha 1 microglobulin/bikunin, membrane-associated protein 17, complement component factor i, transcription factor EC, ectonucleotide pyrophosphatase/phosphodiesterase 3, Similar to apical early endosomal glycoprotein precursor (LOC381352), mRNA, **bone morphogenetic protein 7**, **potassium voltage-gated channel**, delayed-rectifier, subfamily S, member 3, RIKEN cDNA 2010317E24 gene, expressed sequence AI317395, coagulation factor X, Similar to Aldo-keto reductase family 1 member C13, (LOC238465) mRNA, RIKEN cDNA 2600014C01 gene 0 day neonate thymus cDNA, RIKEN full-length enriched library, clone:A430006A04 product:unknown EST, full insert sequence, ---ribosomal protein S15a, RIKEN cDNA 1810015P03 gene, **lecithin-retinol acyltransferase (phosphatidylcholine-retinol-O-acyltransferase)**, **interleukin 1 alpha**, ---, **leukocyte cell-derived chemotaxin 2**, solute carrier family 17 (anion/sugar transporter), member 5, cytochrome P450, family 3, subfamily a, polypeptide 11, glutathione S-transferase, alpha 2 (Yc2), v-erb-b2 erythroblastic leukemia viral oncogene homolog 3 (avian), nuclear receptor subfamily 2, group E, member 3, RIKEN cDNA 9430065F17 gene, **peptidyl arginine deiminase**, type III, fructose bisphosphatase 1, N-acetyl galactosaminidase, alpha, RIKEN cDNA 9530096D07 gene, ---, fibronectin type III domain containing 5, GATA binding protein 4, dopachrome tautomerase, ATPase, class VI, type 11A, S100 calcium binding protein A1

Upregulation	Gene list (M 10e6 crypto infected vs N 10e6 crypto infected)
>100 fold	inactive X specific transcriptsinactive X specific transcriptsserine (or cysteine) proteinase inhibitor, clade A, member 1aRIKEN cDNA 4933439A12 geneinactive X specific transcripts
31-60 fold	N-acetylneuraminate pyruvate lyase
20-30 fold	bone morphogenetic protein 7 glutathione S-transferase, alpha 3 ankyrin repeat and SOCS box-containing protein 11 antigen p97 (melanoma associated) identified by monoclonal antibodies 133.2 and 96.5 coagulation factor X
10-19 fold	folate receptor 1 (adult), claudin 8, secreted phosphoprotein 2, Similar to apical early endosomal glycoprotein precursor (LOC381352), mRNAretinoic acid receptor responder (tazarotene induced) 1, renin binding protein, coagulation factor X, bone morphogenetic protein 7, metallothionein 2, fibroblast growth factor 15, cytochrome P450, family 3, subfamily a, polypeptide 25mucolipin 3

Future directions

1. Run meningeal macrophage IBA-I IHC with co-localization with arginase I and NOS2, as markers of M1 and M2 macrophages, respectively, by confocal microscopy.

2. Increase the number of mice in some experiments that still require more statistical power.

3. Analyze CSF, meninges and brain metabolomics following *Crypto* infection and diets (testing TMAO translocation to the brain and meninges).

4. Run ELISA and WB for BDGF in the PFC from *C. parvum*-infected mice.

6. Run RT-PCRs for TLR, NOD-1 signaling in the meninges, and PFC of *C.parvum*-infected mice.

TMAO affects in the brain following C. parvum infection in mice?

The Journal of Infectious Diseases

MAJOR ARTICLE

Increased Urinary Trimethylamine *N*-Oxide Following *Cryptosporidium* Infection and Protein Malnutrition Independent of Microbiome Effects

David T. Bolick,[1] Jordi Mayneris-Perxachs,[2] Greg L. Medlock,[3] Glynis L. Kolling,[3] Jason A. Papin,[3] Jon R. Swann,[4] and Richard L. Guerrant[1]

[1]Division of Infectious Diseases and International Health, UVA Center for Global Health, University of Virginia, Charlottesville; [2]Technological Unit of Nutrition and Health, EURECAT—Technological Center of Catalonia, Reus, Spain; [3]Department of Biomedical Engineering, University of Virginia, Charlottesville; and [4]Department of Surgery and Cancer, Division of Computational and Systems Medicine, Imperial College London, United Kingdom.

Cryptosporidium infections have been associated with growth stunting, even in the absence of diarrhea. Having previously detailed the effects of protein deficiency on both microbiome and metabolome in this model, we now describe the specific gut microbial and biochemical effects of *Cryptosporidium* infection. Protein-deficient mice were infected with *Cryptosporidium parvum* oocysts for 6–13 days and compared with uninfected controls. Following infection, there was an increase in the urinary excretion of choline- and amino-acid-derived metabolites. Conversely, infection reduced the excretion of the microbial–host cometabolite (3-hydroxyphenyl) propionate-sulfate and disrupted metabolites involved in the tricarboxylic acid (TCA) cycle. Correlation analysis of microbial and biochemical profiles resulted in associations between various microbiota members and TCA cycle metabolites, as well as some microbial-specific degradation products. However, no correlation was observed between the majority of the infection-associated metabolites and the fecal bacteria, suggesting that these biochemical perturbations are independent of concurrent changes in the relative abundance of members of the microbiota. We conclude that cryptosporidial infection in protein-deficient mice can mimic some metabolic changes seen in malnourished children and may help elucidate our understanding of long-term metabolic consequences of early childhood enteric infections.

Keywords. choline; *Cryptosporidium*; malnutrition; metabonome; microbiome.

BMC Syst Biol. 2016 Aug 26;10 Suppl 3:63. doi: 10.1186/s12918-016-0307-y.

Towards understanding brain-gut-microbiome connections in Alzheimer's disease.

Xu R[1], Wang Q[2].

Author information

Abstract

BACKGROUND: Alzheimer's disease (AD) is complex, with genetic, epigenetic, and environmental factors contributing to disease susceptibility and progression. While significant progress has been made in understanding genetic, molecular, behavioral, and neurological aspects of AD, relatively little is known about which environmental factors are important in AD etiology and how they interact with genetic factors in the development of AD. Here, we propose a data-driven, hypotheses-free computational approach to characterize which and how human gut microbial metabolites, an important modifiable environmental factor, may contribute to various aspects of AD.

MATERIALS AND METHODS: We integrated vast amounts of complex and heterogeneous biomedical data, including disease genetics, chemical genetics, human microbial metabolites, protein-protein interactions, and genetic pathways. We developed a novel network-based approach to model the genetic interactions between all human microbial metabolites and genetic diseases. We identified metabolites that share significant genetic commonality with AD in humans. We developed signal prioritization algorithms to identify the co-regulated genetic pathways underlying the identified AD-metabolite (brain-gut) connections.

RESULTS: We validated our algorithms using known microbial metabolite-AD associations, namely AD-3,4-dihydroxybenzeneacetic acid, AD-mannitol, and AB-succinic acid. Our study provides supporting evidence that human gut microbial metabolites may be an important mechanistic link between environmental exposure and various aspects of AD. We identified metabolites that are significantly associated with various aspects in AD, including AD susceptibility, cognitive decline, biomarkers, age of onset, and the onset of AD. We identified common genetic pathways underlying AD biomarkers and its top one ranked metabolite trimethylamine N-oxide (TMAO), a gut microbial metabolite of dietary meat and fat. These coregulated pathways between TMAO-AD may provide insights into the mechanisms of how dietary meat and fat contribute to AD.

CONCLUSIONS: Employing an integrated computational approach, we provide intriguing and supporting evidence for a role of microbial metabolites, an important modifiable environmental factor, in AD etiology. Our study provides the foundations for subsequent hypothesis-driven biological and clinical studies of brain-gut-environment interactions in AD.

Functional Coupling of Human Microphysiology Systems: Intestine, Liver, Kidney Proximal Tubule, Blood-Brain Barrier and Skeletal Muscle

Lawrence Vernetti[1,2,*], Albert Gough[1,2,*], Nicholas Baetz[3], Sarah Blutt[4], James R. Broughman[4], Jacquelyn A. Brown[5], Jennifer Foulke-Abel[3], Nesrin Hasan[3], Julie In[3], Edward Kelly[6], Olga Kovbasnjuk[3], Jonathan Repper[7], Nina Senutovitch[1], Janet Stabb[3], Catherine Yeung[8,9], Nick C. Zachos[3], Mark Donowitz[3,†], Mary Estes[4,†], Jonathan Himmelfarb[9,10,†], George Truskey[7,†], John P. Wikswo[5,11,†] & D. Lansing Taylor[1,2,12,†]

Organ interactions resulting from drug, metabolite or xenobiotic transport between organs are key components of human metabolism that impact therapeutic action and toxic side effects. Preclinical animal testing often fails to predict adverse outcomes arising from sequential, multi-organ metabolism of drugs and xenobiotics. Human microphysiological systems (MPS) can model these interactions and are predicted to dramatically improve the efficiency of the drug development process. In this study, five human MPS models were evaluated for functional coupling, defined as the determination of organ interactions via an *in vivo*-like sequential, organ-to-organ transfer of media. MPS models representing the major absorption, metabolism and clearance organs (the jejunum, liver and kidney) were evaluated, along with skeletal muscle and neurovascular models. Three compounds were evaluated for organ-specific processing: terfenadine for pharmacokinetics (PK) and toxicity; trimethylamine (TMA) as a potentially toxic microbiome metabolite; and vitamin D3. We show that the organ-specific processing of these compounds was consistent with clinical data, and discovered that trimethylamine-N-oxide (TMAO) crosses the blood-brain barrier. These studies demonstrate the potential of human MPS for multi-organ toxicity and absorption, distribution, metabolism and excretion (ADME), provide guidance for physically coupling MPS, and offer an approach to coupling MPS with distinct media and perfusion requirements.

Acknowledgments

To: the Center for Global Health, the Division of Neuroscience, and the BIG Center/UVA

Special thanks:

-Dr. Richard L. Guerrant
-Dr. Cirle Warren
-David Bolick
-Jae Shin

-Pedro Quintela Medeiros
-Deiziane da Silva Costa
-Orleâncio Ripardo de Azevedo
-Ibraim Castro
-Cássia Roque
-Juliana Rego
-Ronaldo P. Dias
-Aldo A.M. Lima
-Gerly A.C Brito